KYAMBOGO UNIVERSITY

SYNTHESIS AND CHARACTERIZATION OF IRON AND NITROGEN CO-DOPED CARBON CATALYST FOR OXYGEN REDUCTION

BY

OLADO SIMON PETER

(BSc. Technology in Chemistry, KyU)

21/U/GMCH/14557/PE

A DISSERTATION SUBMITTED TO KYAMBOGO UNIVERSITY DIRECTORATE OF RESEARCH AND GRADUATE TRAINING IN PARTIAL FULFILLMENT OF THE REQUIREMENTS FOR THE AWARD OF MASTER OF SCIENCE IN CHEMISTRY DEGREE OF KYAMBOGO UNIVERSITY

June 2024

DECLARATION

I, Olado Simon Peter, hereby declare that this submission is my own work and that, to the best of my knowledge and belief, it contains no material previously published or written by another person nor material that has been accepted for the award of any other degree for the University or other institute of higher learning, except where due acknowledgment has been made in the text and reference list.

Signature: …….. Date: …….

APPROVAL

The undersigned approve that they have read and hereby recommend for submission to the Directorate of Research and Graduate Training of Kyambogo University, a dissertation entitled: "Synthesis, characterization and kinetic study of iron and nitrogen co-doped carbon catalyst for electrocatalytic oxygen reduction" in partial fulfilment of the requirements for the award of Master of Science in Chemistry Degree of Kyambogo University.

Dr. Masa Justus (Principal Supervisor)

Signature: ..... **Date:** 17.06.2025.....

Dr. Jude Tadeo Inyalot (Co-Supervisor)

Signature: ..... **Date:** .....

DEDICATION

I dedicate this dissertation to my wife Mrs. Olado Lavin, my parents late Mr. Naloda Joseph and Ms. Kanyago Irene and the family of Mr and Ms. Adotu Robert for their unconditional love and care they have always given to me.

ACKNOWEDGEMENT

I begin by thanking God Almighty for bringing me this far. It has been His Grace that am able to come to this point.

I wish to convey my profound appreciation to my supervisors, Dr. Justus Masa and Dr. Jude Tadeo Inyalot, for their priceless mentorship, unfailing assistance, and motivation during this research undertaking. Their profound knowledge, perceptive and prompt input, and unwavering commitment have played a crucial role in influencing the course of this project and successfully overcoming its obstacles.

I express my gratitude to Kyambogo University and Makerere University (CEDAT) for furnishing the vital resources and facilities required for carrying out this research. I am grateful to my colleagues and friends for their insightful conversations and moral encouragement, which have enhanced my academic progress and helped to the advancement of this dissertation.

Ultimately, I am deeply appreciative of my family for their unwavering affection, support, and forbearance during this undertaking. Their steadfast faith in me has served as my wellspring of fortitude and motivation. This study would not have been feasible without the combined participation and backing of all the individuals listed before.

TABLE OF CONTENTS

LIST OF TABLES

LIST OF FIGURES

LIST OF ABBREVIATIONS

Abbreviation	Full form
E	Electrode potential
CDs	Carbon Dots
CE	Counter Electrode
CoP	Cobalt-Phosphide
CV	Cyclic Voltammetry/Voltammogram
DFT	Density Functional Theory
EDS	Energy Dispersive X-Ray Spectroscopy
EDX	Energy Dispersive X-ray Spectroscopy
EIS	Electrochemical Impedance Spectroscopy
FC	Fuel Cell
FeNC	Iron, nitrogen co-doped Carbon
FWHM	Full Width at Half Maximum
GC	Glassy Carbon
GO	Graphene Oxide
HAADF	High-Angle Annular Dark-Field
HOR	Hydrogen Oxidation Reaction
IPA	Isopropyl Alcohol
KPI	Key Performance Indicators
LR	Laboratory Reagent Grade
LSV	Linear Sweep Voltammetry/Voltammogram
MC	Metal Carbide
MNC	Metal and Nitrogen co-doped Carbon
MOFs	Metal Organic Frameworks
NC	Nitrogen-doped Carbon

OER	Oxygen Evolution Reaction
ORR	Oxygen Reduction Reaction
OSS1	Iron, nitrogen co-doped Carbon (nitrogen source-egg album)
OSS2	Iron, nitrogen co-doped Carbon (nitrogen source-caffeine)
PEMFCs	Proton Exchange Membrane Fuel Cells
PGM	Platinum Group Metals
PRR	Peroxide Reduction Reaction
Pt/C	Platinum on Carbon
PTFE	Polytetrafluoroethylene
RDE	Rotating Disk Electrode
RDS	Rate Determining Step
RE	Reference Electrode
RRDE	Rotating Ring Disk Electrode
SDGs	Sustainable Development Goals
SEM	Scanning Electron Microscopy
TEM	Transmission Electron Microscopy
UN	United Nations
UNDP	United Nations Development Programme
WE	Working Electrode
XPS	X-ray Photoelectron Spectroscopy
XRD	X-ray Diffraction

ABSTRACT

Global pollution and global warming (climatic change) predominantly result from over dependence on fossil fuels. This has been exacerbated by increasing demand for energy driven by rising global population and industrialization. Renewable energy sources can reduce the environmental impact of fossil fuels and other non-environmental systems, thus drawing global interest. Due to their low CO_2 emissions, fuel cells and metal-air batteries are preferred energy systems to replace fossil fuels. But the slow Oxygen Reduction Reaction and Oxygen Evolution Reaction in fuel cells and metal air batteries during discharge and charging make these technologies difficult. For fuel cells and metal air batteries to advance, efficient and cost-effective electrocatalysts are needed for the ORR half-reaction.

This study developed an efficient and cost-effective iron and nitrogen co-doped carbon electrocatalyst as an alternative to platinum-based ORR catalysts. The catalyst was prepared pyrolysing caffeine and egg albumen as the nitrogen-rich biomass source, graphite powder as a support matrix, and Iron (III) chloride hexahydrate as the Fe source and pyrolyzing at 850 ^{o}C. The catalysts, OSS1 for egg albumen and OSS2 for caffeine, were characterised using X-ray diffraction and SEM with EDX. The synthesised catalysts' electrocatalytic characteristics were examined using Rotating Disc Electrode in oxygen saturated in 0.1 M KOH in a three-electrode cell configuration with silver electrode as the reference electrode. The catalyst prepared with caffeine as the nitrogen source (OSS2) had the most promising ORR activity, with a higher kinetic current of 2.189 mA cm^{-2} at -0.466 V and a selectivity of oxygen reduction to water via hydrogen period pathway (n = 3.24)

predominantly via the 4-electron pathway, Tafel slope of 114.650 $mVdec^{-1}$, and exchange current density of 0.459 $mAcm^{-2}$. OSS1 had a slightly lower kinetic current of 1.609 mA cm^{-2} at -0.433 V. Finally, Graphitic Carbon showed a reduced kinetic current of 1.007 mA cm^{-2} at -0.290 V, selectivity of oxygen reduction to water via peroxide pathway (n = 2.38), Tafel slope of 95.920 $mVdec^{-1}$, and exchange current density of 0.354 $mAcm^{-2}$. The electron transfer number of the catalysts differed significantly (p = 0.001), indicating that the nitrogen supply significantly affects ORR activity. Thus, the results demonstrate the impact of biomass-derived nitrogen precursor characteristics on Fe-N-C catalyst for oxygen reduction.

Keywords: Oxygen reduction reaction, iron-nitrogen co-doped carbon, rotating ring electrode.

CHAPTER ONE

INTRODUCTION

1.1. Background to the study

Due to their environmental friendliness, fuel cells (FCs) and metal-air batteries (MABs) are very appealing energy systems for reducing global challenges brought on by the use of non-renewable energy (Kulkarni *et al*., 2018; Feng *et al*., 2021). FCs are energy conversion systems that continually generate power by harnessing the electrons released from the reaction of a fuel and an oxidant (Shao *et al*., 2016). Numerous industries, offices and domestic buildings can benefit from the use of fuel cells (Chadly *et al*., 2022).

The Oxygen Reduction Reaction (ORR) is a key reaction in FCs and is a limiting reaction in MABs and FCs (Debe, 2012; Dou *et al*., 2020). The best ORR catalysts known are Pt and Pt-based materials (Peng *et al*., 2013). Nevertheless, the extensive adoption of these materials in practical devices has been significantly hindered by their exorbitant expense, scarce natural availability, inadequate longevity, and limited capacity to tolerate methanol, among other factors (Li *et al*., 2019a; Vij *et al*., 2016; Yang *et al*., 2022). The presence of methanol is unwanted due to its tendency to poison catalytic sites when ORR is carried out on Pt-based and most Pt group catalysts (Amani et al., 2015). For example, Toyota Mirai, a commercially available hydrogen FC vehicle goes for about 57,000 US dollars in the North American market. The outrageous cost of the Toyota Mirai is strongly associated with the substantial platinum loading in the fuel cell (Shao *et al*., 2016).

It is imperative to guarantee universal access to affordable, dependable, sustainable, and contemporary energy in accordance with the United Nations Sustainable Development Goal 7 (Sustainable & Goals, 2021). There have been tremendous efforts undertaken to lower catalyst costs by alloying Pt with non-noble metals (Shen *et al*., 2019; Wang *et al*., 2022).

There are three requirements that FCs and MABS technologies must satisfy in order to achieve industrial applications, which include; cost, performance, and durability (Wang *et al*., 2021a). The other challenge associated with FCs is that the anode reaction, that is, Hydrogen Oxidation Reduction (HOR), in the case of hydrogen FCs, is six times faster than the cathode reaction, the ORR, which limits the FCs performance. Most of the research and development efforts are directed at enhancing the performance of cathode catalysts and electrodes (Dincer, 2007).

In Uganda, Platinum is found in Nakiloro, located 16 km northeast of Moroto town and Nakiloro is considered as a significant area for potential platinum deposits. This platinum deposit is associated with chromite prospects in chlorite schists. But this chromite has not been produced to date (MEMD, 2020).

Non-Pt nano-hybrids, on the other hand, have garnered increased attention due to their encouraging ORR activity and lower costs. Metal-Nitrogen-doped carbon (MNC) nanostructures have been identified as one of the most promising potential alternatives to Pt-based ORR catalysts (Jiang *et al*., 2016; Masa *et al*., 2015; Masa *et al*., 2013). For fuel cell devices to become commercially feasible, a substantial decrease in cost is required. In order to enhance the competitiveness of FCs stacks, it is imperative to decrease the

expenses associated with materials and production of stack components. Additionally, the prices of high-performance membranes and catalysts must be reduced (Cells *et al.*, 2016).

1.2. Statement of the problem

Energy is a global domestic and industrial need and it is one of the biggest drivers of development and technological advancement. The currently most used energy source is fossil fuels, which have resulted in global pollution. To negate these effects, there is need to develop sustainable energy systems. FCs and MABs have been developed as promising energy systems that can significantly contribute to abatement of problems associated with the use of fossil fuels. FCs, particularly hydrogen fuel cells, have net zero CO_2 emissions when fed with green hydrogen. Metal-air batteries exhibit theoretically higher energy densities than conventional batteries.

The major drawback of these technologies is slow kinetics of the ORR, a key cathodic reaction in both technologies. The most powerful catalysts for ORR, are either Pt or platinum-based composites and its alloys. The scarcity and high costs associated with Pt and its derivatives has made commercialization of FCs and MABs technologies uneconomical. Transition metals like Fe, Co, and Ni as well as their composites with nitrogen-doped carbon materials have been explored as potential alternatives to Pt for ORR and Ru and Ir for OER. Platinum catalysts have a tendency of suffering inevitable deactivation due to the migration and strong adsorption of anions and methanol onto the catalyst.

Pure iron has a comparatively high oxygen binding energy compared to Pt. However, this favours adsorption of oxygen but not desorption of products containing oxygen which

necessitates regulation of this binding energy. This can be achieved by developing catalysts in which Fe is coordinated to dopants like nitrogen (N), sulphur and phosphorus, among others, to modulate the binding energy of oxygen and oxygen reduction intermediates on the Fe sites. Additionally, iron is highly abundant and readily accessible, which would potentially such Fe-based catalysts cost-effective and scalable. This work sought to synthesize iron and nitrogen co-doped carbon (Fe-N-C) catalysts for electrocatalytic oxygen reduction using egg albumen and caffeine as biomass based carbon and nitrogen sources

1.3. Objectives of the study

1.3.1. General objective

The general objective of this study was to synthesise and characterize iron nitrogen co-doped catalyst and investigate their kinetics of electro-catalytic oxygen reduction reaction.

1.3.2. Specific objectives

i. To prepare iron nitrogen co-doped carbon catalysts.

ii. To characterise the synthesised iron nitrogen co-doped carbon catalysts.

iii. To determine electrocatalytic performance of the synthesized iron nitrogen co-doped carbon catalysts for ORR.

1.4. Justification

Iron-based electrocatalysts have been shown to be promising alternatives to platinum-based catalysts due to their lower cost and good performance (Shen *et al.*, 2019). Introducing N functionalities in carbon structure, specifically pyrrolic, pyridinic, and graphitic N groups, along with iron, into carbon has demonstrated the ability to create highly effective

electrocatalysts. However, most nitrogen sources pyridine (Xia *et al*., 2011), pyrrole (Chen *et al*., 2021; Jiménez-Ramírez *et al.*, 2017; Lilloja *et al*., 2021) and melamine (Liu et al., 2022) reported are of fossil origin. There is need to study possible renewable alternatives These electrocatalysts are now the top candidates for replacing platinum in ORR applications (Feng *et al*., 2013; Wei *et al*., 2015). Additionally, caffeine (Rameshaiah & Ashoka, 2015) and egg albumen (Chiralt et al., 2017) are rich in nitrogen and could be a good source of nitrogen as a dopant.

1.5. Significance

i. This study is expected to contribute to the development of improved, cost-effective catalysts for more efficient and economical energy storage and conversion technologies.

ii. The results obtained from this study has the capacity to generate significant progress in the domain of electrocatalysis and the development of environmentally stable energy systems. These developments may have a positive impact on both the environment and society as a whole.

iii. This research significantly advances Sustainable Development Goal (SDG) 7 by tackling essential hurdles in clean energy technology through the creation of effective, non-precious metal electrocatalysts for fuel cells. Optimising nitrogen-doped carbon-based catalysts for the Oxygen Reduction Reaction (ORR) immediately facilitates the shift to cost-effective and sustainable energy systems.

1.6. Scope of the study

The scope of the study was limited to synthesis of the Fe-N-C electrocatalyst using wet impregnation and thermal treatment methods, and to characterize them using a range of methods such as X-ray diffraction (XRD) and scanning electron microscopy (SEM) integrated with Energy Dispersive X-ray spectrometry (EDX). The ORR activity of the Fe-N-C electrocatalyst will be studied using the rotating disk electrode (RDE) voltammetry technique and linear sweep voltammetry (LSV) to determine, the onset potential, kinetic current, exchange current density, electrons transfer number (n), reaction rate constant and electron transfer coefficient (α). The reaction was investigated in an alkaline electrolyte potassium hydroxide (0.1M) saturated with oxygen. The work was conducted from October 2022 to June 2024 at the Department of Chemistry research laboratory, Kyambogo University (Kampala), while characterization of the synthesized materials was conducted at Makerere University in the Material Science Laboratory.

1.7 Conceptual framework

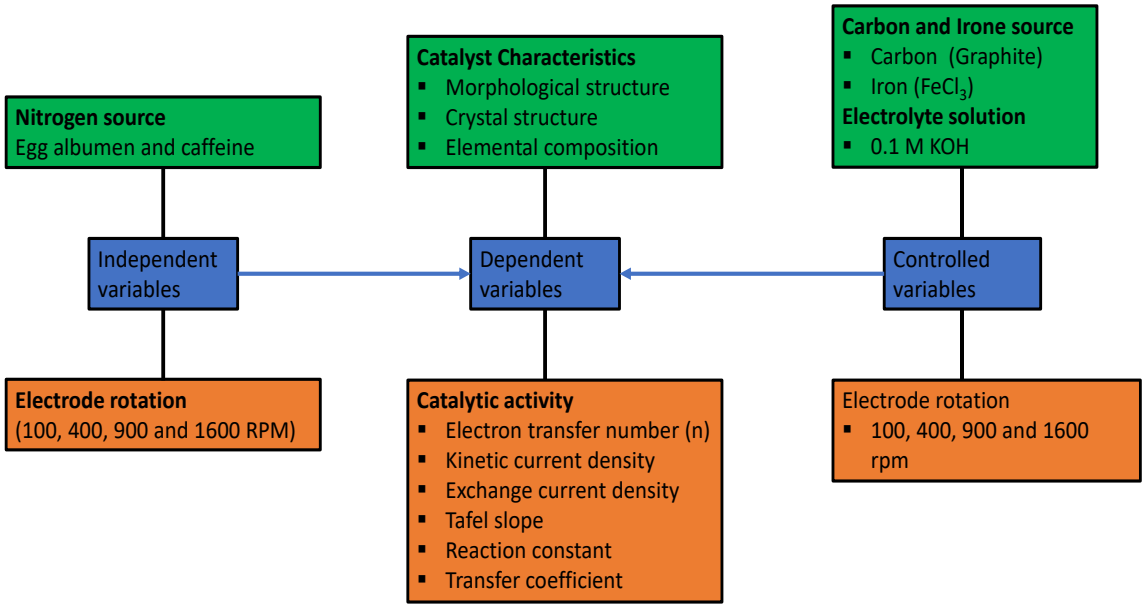

Figure 1.1: The conceptual framework of the study

CHAPTER TWO

LITERATURE REVIEW

2.1. Fuel cells

Fuel cells (FCs) are electrochemical devices that transforms fuel and oxidant into electrical energy and heat energy. Hydrogen (H_2) FCs, which rely on H_2 as the fuel and oxygen (O_2) from the atmosphere as the oxidant, are the predominant and extensively researched category of fuel cells. The processes occurring in a hydrogen FCs are the inverse of water electrolysis, when an electric current decomposes water into its basic elements, H_2 and O_2. Hydrogen FCs facilitate a reaction between H_2 (fuel) and oxidizer (air or O_2) at the anode and cathode, respectively. This process results in the production of electricity, heat, and water (Shao *et al*., 2016). When the fuel and oxidant are continually supplied, FCs and MABs generate electric energy continuously, unlike batteries which store energy (Shah, 2007).

Fuel cells offer a great prospect to obtain cleaner, green and more sustainable energy supply in the 21st century and beyond with the potential to significantly reduce CO_2 emission thus aiding towards achievement of the United Nations (UN) climatic goals of net-zero CO_2 emissions by 2050. There exist several FCs mostly categorised based on the electrolyte or fuel type, although all of them require ORR as the cathode reaction (Wei *et al*., 2015).

2.2. The oxygen reduction reaction (ORR)

The ORR is a chemical process that involves reduction of oxygen to water. In FCs and MABs, ORR is the half-cell reaction that converts oxygen gas at the cathode into water as illustrated in the following chemical equations in alkaline and acidic media respectively. Depending on the

catalyst used, a 4 or 2 electron pathway mechanism is adopted with the former being for perfect catalysts.

In alkaline media

$$O_2 + 2H_2O + 4e^- \rightarrow 4OH^-$$

or

$$O_2 + H_2O + 2e^- \rightarrow HO_2^- + OH^-$$

$$HO_2^- + H_2O + 2e^- \rightarrow 3OH$$

In acidic media

$$O_2 + 4H^+ + 4e^- \rightarrow 2H_2O$$

or

$$O_2 + 2H^+ + 2e^- \rightarrow H_2O_2$$

$$H_2O_2 + 2H^+ + 2e^- \rightarrow 2H_2O$$

Many energy storage and transformation technologies, such as MABs and FCs, depend on the ORR as the cathode reaction (Wang *et al.*, 2021b).

The other half-cell reaction in a FCs (anodic reaction) hinge on the type fuel or FC. For the hydrogen FCs, the anode reaction is the HOR. The ORR is a critical reaction in FCs, as it influences the overall kinetics, efficiency and performance of the cell (He and Cairns, 2015; Masa *et al.*, 2014; Masa *et al.*, 2013).

The cathode of the hydrogen FC is typically comprised of a porous or etched structure to enable oxygen transport to the inner catalyst surface. Additionally, it acts as the current collector relaying electrons between the catalyst and the external circuit. At the cathode, the electrons associate with oxygen and hydrogen ions from the oxidation of hydrogen at the anode, to form water. There are numerous pathways and processes during the ORR, including direct and

indirect mechanisms (Shah, 2007). In the direct mechanism, the ORR takes place at the cathode surface and its kinetics are directly influenced by the electrode surface properties. In the indirect mechanism, the ORR happens via mediation by surface species, such as hydroxyl or hydroperoxyl groups (He and Cairns, 2015).

2.2.1. Mechanism of the ORR

At room temperature (20-25°C), protons (H^+) and 2 or 4 electrons can reduce oxygen which is a gas in an aqueous solution resulting in production of hydrogen peroxide (H_2O_2) or water, respectively, as summarized in Table 2.1. The superoxide radical anion ($O_2^{\bullet}$) is generated after one electron reduction of molecular O_2, followed by two electron reduction to form H_2O_2 in acidic electrolytes or the hydroxyl radical ($OH^{\bullet}$) in alkaline electrolytes, and four electron reduction to form water.

Oxygen reduction occurs in non-aqueous solutions by accepting one electron, and the electrode potential is determined by the kind of solvent utilized (Wood, 1988). The ORR in MABs is very appealing due to their superior energy density and specific capacity than to conventional batteries (Inamuddin *et al*., 2020).

Although both the ORR and its counter-part, the HOR, are kinetically faster in acidic electrolytes, in part due to the ideally higher ionic conductivity of the proton owing primarily to its comparatively smaller size compared to the hydroxide anion in alkaline electrolytes, alkaline media are preferred due to the prospect of using non-platinum group metal-based catalysts.

Table 2.1: The mechanism of ORR in acidic and alkaline media

Acidic medium	E(V)	Alkaline medium	E(V)
$O_2 + 4H^+ + 4e \rightarrow 2H_2O$	1.23	$O_2 + 2H_2O + 4e^- \rightarrow 4OH^-$	0.401
$O_2 + 2H^+ + 2e \rightarrow H_2O_2$	0.70	$O_2 + H_2O + 2e^- \rightarrow HO_2^- + OH^-$	-0.065
$H_2O_2 + 2H^+ + 2e^- \rightarrow 2H_2O$	1.76	$HO_2^- + H_2O + 2e^- \rightarrow 3OH^-$	0.867

Despite the sluggish kinetics of the ORR, it is always necessary to have a highly efficient and stable catalyst to expedite the electrochemical phenomena. Platinum metal supported on carbon is now considered the exemplary or cutting-edge ORR electrocatalyst with excellent activity and efficiency. Expensive and limited availability of Pt metal motivate researchers to seek for cheaper alternative catalysts for ORR (Inamuddin *et al*., 2020).

For FC applications, it is essential to have a catalyst that produces none or very little H_2O_2 during the ORR. The 4-electron O_2 reduction pathway can occur by either a direct 4e- or a consecutive 2e− x 2e− mechanism on a single active site (Gewirth *et al*., 2018). Similarly, an alternate theory involves the participation of two active sites in a bifunctional process that requires the transfer of two electrons at each individual site. Therefore, including additional active sites to facilitate further peroxide reduction reaction (PRR) is a logical strategy to address the challenges related to the generation of H_2O_2. Fe-N-C catalysts tend to exhibit ORR reactivity towards both the $2e^-$ and $4e^-$ pathways leading to the formation of intermediate H_2O_2 in an alkaline solution. However, the presence of multiple possible active sites in the Fe-N-C catalysts, including Fe-N-C centres, nitrogen functional groups, and Fe_2O_3, can act concertedly to reduce H_2O_2 further to water. The presence of Fe_2O_3, a potent catalyst for H_2O_2 disproportionation, parallelly contributes to elimination of any formed H_2O_2. Therefore, with a well-optimized composition, Fe-N-C catalysts inherently contain secondary active sites to

further reduce H_2O_2 produced during the ORR to water via a 2e− + 2e− mechanism. Consequently, a well-optimized Fe-N-C catalyst comprising a high density of Fe-N-C centres, the moieties that are believed to support the direct 4e⁻ pathway, and the additional sites comprised of nitrogen functional groups (pyridinic, pyrrolic and graphitic), defect sites on carbon, Fe_2O_3, and surface groups, is expected to exhibit excellent efficiency in reducing O_2, with improved selectivity and endurance.

2.3. Electrocatalysis

A catalyst is a substance that accelerates a reaction's rate with itself not being destroyed in the process. Depending on whether it is in the same phase as the reactant or not, a catalyst can be homogeneous or heterogeneous respectively. Heterogeneous catalysts offer an alternative low energy pathway from reactants to products. The finest catalytic surfaces will have a reactivity that is selective in terms of reactivity for a particular reaction (Laursen *et al*., 2011).

Electrocatalysts are catalysts that catalyse electrochemical reactions. Typically, transition metal elements and their derivatives like alloys, metal complexes, metal oxides, sulphides, carbides, nitrides, and phosphides are used as electrocatalysts (Serhan *et al*., 2019; Wang *et al*., 2021; Zhao *et al*., 2019).

There is need to replace fossil fuels with non-CO_2 emitting renewable energy such as sunlight and wind, there are electrochemical systems that transforms renewable energy into portable fuels and chemicals as a means for energy storage. Conversely, systems that convert fuels back to electricity, are expected to play a central role in reducing net CO_2 emissions in future energy systems. Electrocatalysis is crucial in both systems that inter-convert electricity into

fuels and chemicals, and vice versa, that is, fuels back to electricity. This calls for the design of catalysts that can favour desired products with the least overpotential or voltage possible while ensuring the most durable performance (Lei *et al*., 2022). Overpotential is the additional voltage, above the thermodynamic equilibrium potential, necessary to facilitate an electrochemical reaction at a specific rate (Appel & Helm, 2014).

The principle that governs the catalytic properties of solid surfaces is the Sabatier Principle (Laursen *et al*., 2011). According to this principle, the reactants must have a significant affinity for the catalyst surface in order to form reaction intermediates. However, this affinity should be not as strong as to prevent detachment of the products from the catalyst surface, thereby facilitating subsequent reactions at the reaction sites.

The catalyst loading has a huge impact on fuel cell costs. Fuel cell engineers strive to keep cell efficiency high while using as little platinum as possible (Alonso-Vante *et al*., 2019).

Transition metals are widely used as electrocatalysts, however, due to their very strong binding energies for oxygen and the ORR reaction intermediates, O^*, OH^*, and OOH^*, they are not suitable for ORR electrocatalysis. This work has shown that modifying carbon with controlled amounts of transition metals and N generates novel catalysts for ORR as reported by (Masa *et al*., 2013).

2.4. Carbon-based electrocatalysts for ORR

Carbon-based catalysts are widely used because they are versatile, inexpensive, and have adjustable chemical structures. This section examines the chemical compositions of various carbon-based catalysts and their effect the activity and selectivity of the ORR.

2.4.1. Graphene-based catalysts

Graphene consists of a monolayer of carbon organised in a hexagonal lattice. The planar configuration offers a great surface area and exceptional electrical conductivity, which are crucial for electrocatalysis of the ORR (Zhang *et al*., 2021). Nitrogen doping is a prevalent method employed to alter the active sites of carbon-based catalysts and to incorporate new active sites comprised of N functional groups for ORR. Nitrogen is introduced into the carbon structure, resulting in the formation of pyridinic, pyrrolic and graphitic nitrogen. The presence of nitrogen species has the ability to modify the interaction with oxygen molecules, hence promoting the ORR via the 4-electron O_2 reduction pathway (Wang *et al*., 2022). The N-based functional groups augment the electron density at the active sites, hence enhancing electrocatalytic activity.

2.4.2. Carbon nanotubes (CNTs)

Carbon nanotubes are carbon structures with a cylindrical shape and are made up of graphene sheets that are rolled into tubes. CNTs can exist in two forms: single-walled or multi-walled, and they can vary in terms of their diameters and lengths. Due to their exceptionally high surface area, conductivity and ability to be modified with heteroatoms, they are well-suited for applications involving the ORR. The introduction of heteroatoms such as N into CNTs generates active sites that have the possibility of increasing the ORR activity (Wei *et al*., 2020). Nitrogen-doped CNTs can have N atoms located at either pyridinic or pyrrolic sites (as illustrated in figure 2.1), which in turn affects the catalyst's selectivity towards either the 2 or 4e pathway. Pyridinic N is typically linked to selectivity for the 4e pathway, whereas pyrrolic N are reported to favour the 2e selectivity (Kim *et al*., 2019).

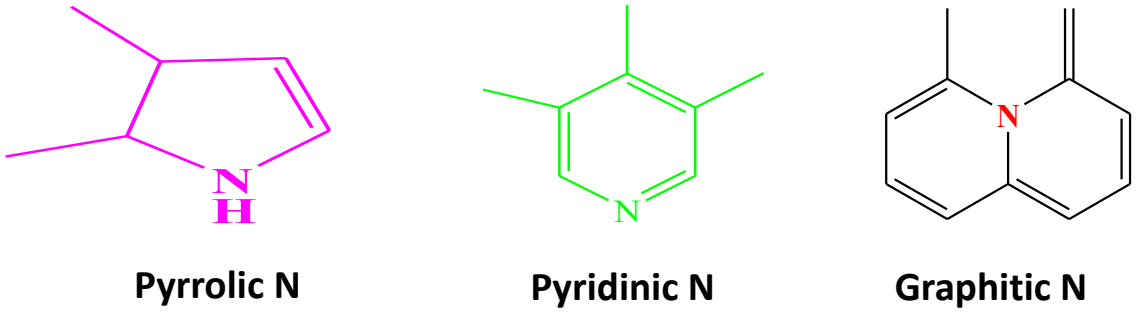

Figure 2.1: The types of nitrogen doped on carbon.

Carbon nanofibers are composed of carbon atoms organized in a fibrous arrangement, providing a large surface area and excellent electrical conductivity. Heteroatoms or supported metal complexes can be used to modify the chemical structure of CNFs (Chen *et al*., 2019). Introducing N into CNFs generates reactive sites that can enhance the ORR, with graphitic N playing a major role in promoting the 4e route. Carbon nanofibers are frequently employed as support materials for metal-nitrogen complexes. The unique chemical structure of the carbon fibers facilitates efficient electron transfer during the ORR, leading to enhanced catalytic activity and selectivity.

Carbon dots, often abbreviated as CDs, are carbon particles at the nanoscale that possess distinctive optical and electrical characteristics. Their structure is approximately spherical and the surface can be adjusted to modify their chemical properties (Abbo *et al*., 2021). Carbon dots can be chemically modified by including heteroatoms like nitrogen or sulphur, which generates active sites for the ORR (Shen *et al*., 2021; Xu *et al*., 2023). The addition of N to CDs possess high activity and ORR selectivity (Miao *et al*., 2020), by increasing the electron density at the active sites, resulting in preferential ORR reduction via the 4e pathway.

Graphene oxide is produced by oxidizing graphene (Shilpa *et al*., 2018; Zhou *et al*., 2020; Zou *et al*., 2016), leading to the formation of oxygen-containing functional groups like carboxyl, hydroxyl, and epoxide (Alam *et al*., 2017). These groups have the potential to greatly influence the ORR activity by serving as active sites and potential adsorption sites for oxygen (Wang *et al*., 2021). Heteroatom doping or reduction procedures can be used to modify the chemical structure of GO, resulting in the development of additional active sites. Sulphur and Nitrogen doping are often employed to augment ORR activity and selectivity for the 4e pathway in GO based catalysts (Xu *et al*., 2020). Besides the ORR, the distinctive configuration of GO, characterized by its oxygen functional groups, enables a diverse array of uses in catalysis.

Activated carbon is a form of high surface area carbon, created through physical or chemical activation processes (Duan *et al*., 2023). The chemical structure of activated carbon offers a large number of pores, allowing for efficient diffusion of reactants and products during the ORR (Wu *et al*., 2015). AC is regularly used as a support material for M-N-C catalysts (Gewirth *et al*., 2018; Miao *et al*., 2020), where the interaction between transition metals and N creates active sites for the ORR. The high porosity and conductivity of activated carbon facilitate electron transfer and increase the concentration of active sites per unit area, thereby contributing to high catalytic turnover.

2.4.3. Carbon-supported metal catalysts

Carbon-supported metal catalysts consist of metal nanoparticles that are deposited onto a carbon matrix (Gewirth *et al*., 2018). The carbon matrix's chemical structure offers stability

and conductivity, while the metal nanoparticles act as active sites for the ORR (Tohnoe *et al*., 1989). Pt-based catalysts reinforced on carbon are frequently used because of their high ORR activity and their preference for the 4e pathway. The interaction between the metal NPs and the carbon matrix generates advantageous electronic characteristics, resulting in enhanced catalytic efficacy (Masa *et al*., 2013).

In addition, non-precious metal catalysts supported or embedded in carbon, such as Fe and Co, can also exhibit enhanced ORR activity. The presence of a carbon matrix further improves the stability, longevity and cost of these catalysts (Yang *et al*., 2021). The chemical composition of the carbon support plays an important role in determining the activity and selectivity of these catalysts.

2.5. Heteroatom-doped carbon catalysts for the ORR

Doping heteroatoms with various electron configurations, atomic sizes, and electronegativities into carbon modifies the surface physicochemical characteristics of carbon and hence their electrocatalytic properties. Three dopants that are frequently used are nitrogen (Masa *et al*., 2013), sulphur , and boron (Sun *et al*., 2015). Doping carbon with any of these atoms improves the electronic properties of the carbon (Wiggins-Camacho and Stevenson, 2011). The change in electronic properties can be elucidated by increase of the I_D/I_G ratio, where I_D and I_G are the peak intensities of the D and G Raman bands, respectively, of carbon (Liu *et al*., 2022). As a result of the difference in electronic configurations and electronegativities, there is transfer of electrons from atom of lower electronegativity to that of higher electronegativity which changes the adsorption capacity of the reaction

intermediates on the electrocatalyst thus boosting the electrocatalytic activity (Sun *et al*., 2015).

2.5.1. Nitrogen-doped carbon catalysts

Nitrogen is the predominant heteroatom employed for doping carbon-based catalysts. Nitrogen doping generates active sites that enhance the ORR activity and can impact the selectivity for either the 2-electron or 4-electron pathway. The nitrogen in N-doped carbon can have various N structures, such as pyridinic, pyrrolic, and graphitic N (Jiménez-Ramírez *et al*., 2017). Pyridinic N (N atom bonded to two carbon atoms inside the hexagonal carbon lattice), is frequently linked to enhanced ORR activity as a result of its electronic characteristics (Xia *et al*., 2011). Research has indicated that pyridinic N has a propensity to favour the 4-electron ORR pathway, resulting in direct reduction to water (Wu and Zelenay, 2013). This characteristic makes it highly desirable for FCs. Graphitic N, which refers to the incorporation of N into the carbon plane, has the ability to improve conductivity as well as the ORR activity.

2.5.2. Sulfur-doped carbon catalysts

Sulphur (S) doping in carbon-based catalysts introduces distinct active sites which potentially influence the activity of the ORR (Kicin and Szala, 2013). Sulphur doping modifies the electronic properties of the neighbouring carbon atoms hence improving the ORR catalytic activity (Zhang et al., 2021). Thiophenic structures can be created by substituting carbon atoms in the hexagonal lattice with sulphur atoms. The presence of these thiophenic sulphur atoms can have a considerable influence on the ORR activity, typically promoting the 4-

electron pathway (Liu *et al*., 2021). Sulphur doping significantly improves the ORR performance in alkaline environments. This is because the increased electron density resulting from sulphur doping enhances the efficiency of oxygen adsorption and reduction.

2.5.3. Boron-doped carbon catalysts

The unusual electrical characteristics of carbon-based catalysts have attracted interest due to the use of Boron (B) as a dopant. Boron atoms can generate electron-deficient regions inside the carbon lattice, which promote the adsorption and reduction of oxygen. Boron's inclusion in the carbon structure can boost the ORR activity, typically promoting the 4-electron pathway (Fazio *et al*., 2014). This is attributed to the favourable interaction between boron-doped sites and oxygen, as reported by Li *et al*. (2022). Boron-doped carbon catalysts have high efficacy in acidic environments, offering a promising substitute for precious metal catalysts in fuel cells (Byeon *et al*., 2023).

2.5.4. Phosphorus-doped carbon catalysts

Phosphorus (P) doping introduces distinct active sites that can improve ORR activity in carbon catalysts (Wang *et al*., 2021a). Phosphorus atoms have the ability to substitute carbon atoms in the hexagonal lattice, resulting in the formation of structures similar to phosphine. These structures have a role in influencing the ORR selectivity (Strelko *et al*., 2000). Phosphorus-doped carbon catalysts have demonstrated significant catalytic activity and selectivity for the 4-electron route, particularly in alkaline environments (Mbokazi *et al*., 2024). Phosphorus enhances the intrinsic activity and hence turns over frequency of the active sites, resulting in enhanced catalytic performance.

2.5.6. Transition metal and nitrogen-doped carbon (MNC) catalysts

Transition MNC catalysts have become a highly interesting category in ORR electrocatalysis. These catalysts, which consist of carbon modified with N in a controlled amount, typically less than 5 wt.%, of various transition metals like Co, Ni, Cu, and Fe, have very promising catalytic ORR activity and provide a cost-effective substitute for precious metals such as platinum (Dou *et al*., 2020).

These catalysts are commonly obtained through the pyrolysis of N rich organic complexes, like metalloporphyrins, metallophthalocyanines and metal-organic frameworks (MOFs), among others, supported on high surface activated carbon, or by directly impregnating carbon supports with a suitable transition metal salt and a N rich organic compound, such as urea, melamine, and subjecting the mixture to fast pyrolysis (Dou *et al*., 2020). The carbon matrix ensures high conductivity, while the incorporated transition metals and N react to generate new kinds of ORR active sites, namely, transition metal coordinated to N and carbon (M-NC), metal carbide (MC) and nitrogen-doped carbon (NC) functional groups.

Metal-nitrogen coordination is a prevalent structural characteristic in which transition metals form bonds with N atoms within the carbon lattice. The arrangement described here generates a high density of ORR active sites, which enhances the catalytic performance (Wu *et al*., 2021). Moreover, transition metals have the ability to generate electronic states inside the carbon structure, which improve the electrons transfer and improve the ORR kinetics.

Extensive research has been conducted on the incorporation of Co into carbon-based materials for ORR electrocatalysis. The presence of cobalt-nitrogen coordination results in

the formation of Co-NC active sites, leading to enhanced ORR activity and selectivity for the 4-electron pathway. The catalysts exhibit high ORR efficacy in alkaline environments, benefiting from the stability and conductivity of cobalt, which leads to improved performance (Shi *et al*., 2022).

Nickel and nitrogen co-doping creates distinct active sites for ORR. The presence of nickel-nitrogen coordination inside the carbon matrix increases the ORR activity, typically promoting the 4-electron pathway (Liu *et al*., 2021). Nickel and nitrogen co-doped carbon catalysts provide exceptional endurance and stability, rendering them well-suited for long-term utilization in fuel cells.

Copper (Cu) in carbon-based catalysts creates more active sites for the ORR. The incorporation of Cu and nitrogen into carbon has been reported to form active structures for ORR activity with preferential selectivity for 4-electron pathway benefitting from the interaction between copper atoms and N. Copper-doped carbon catalysts exhibit efficacy in catalyzing the ORR in both acidic and alkaline electrolytes (Volperts *et al*., 2023).

Transition metal-doped carbon catalysts demonstrate significant ORR efficiency and selectivity for the 4e pathway, which is crucial for FCs utilization. The distinctive active sites formed by the coordination of transition metals and N play a crucial role in facilitating the adsorption and subsequent reduction of oxygen, predominantly via the 4-electron reduction pathway (Masa *et al*., 2015).

2.5.7. Co-doping of heteroatoms in carbon catalysts

The incorporation of numerous heteroatoms in carbon catalysts through co-doping can result in synergistic effects that improve the ORR activity and selectivity. Research has demonstrated that nitrogen-sulphur co-doping enhances the creation of more active sites and boosts electron density, leading to enhanced ORR performance (Alom *et al*., 2023; Shen *et al*., 2023; Strelko *et al*., 2000; Zou *et al*., 2019). The interplay between various heteroatoms can impact the electrical characteristics of the carbon structure, resulting in enhanced oxygen adsorption and reduction efficiency. Co-doping is a favourable method to improve the ORR activity and selectivity of carbon based electrocatalysts in both acidic and alkaline electrolytes.

2.6. Iron-nitrogen co-doped carbon catalysts

Iron and nitrogen co-doped carbon (Fe-N-C) catalysts have emerged as an important class of catalysts, particularly for applications in energy conversion and environmental protection. These catalysts are primarily known for their potential in ORR electrocatalysis, which is crucial for FCs and MABs. The development of Fe-N-C catalysts has been driven by the need for more sustainable and cost-effective alternatives to precious metal catalysts, such as platinum (Gong *et al*., 2009; Maboya *et al*., 2022; Strickland *et al*., 2016; Vij *et al*., 2016; L. Zhao *et al*., 2019).

The practice of introducing heteroatoms such as N and transition metals into carbon compounds has been in existence for several decades (Miao *et al*., 2020). The initial studies conducted in the 1970s and 1980s had a primary focus on comprehending the characteristics

of the carbon catalyst that were doped with nitrogen. Yeager (1984) explored the likelihood of using non-precious metal catalysts for ORR in alkaline environments. This work laid the foundation for further investigations on Fe-N-C catalysts (Yeager, 1984).

During the late 1980s and early 1990s, researchers-initiated investigations on the combined effects of iron and nitrogen co-doping, aiming to uncover any synergistic outcomes. According to the studies done by Yeager in 1964 and later by Yeager and his team showed that the addition of transition metals, such as iron, to nitrogen-doped carbon matrices greatly improved their ability to catalyze the ORR.

In the 2000s, there was tremendous progress in the creation and examination of Fe-N-C catalysts driven by advances in material characterization and better understanding of the ORR reaction mechanism. Several synthesis techniques, such as high-temperature pyrolysis and template-assisted methods, were devised to produce ORR catalysts that are both more active and stable. Lefevre and colleagues made notable contributions during this period, showcasing the significance of precursor composition and pyrolysis conditions on catalytic performance (Lefevre *et al.*, 2000).

Furthermore, advanced analytical techniques have provided deeper insights into the nature of the active sites in Fe-N-C catalysts. These studies revealed that the catalytic activity was often associated with Fe-N_x sites embedded within the carbon matrix (Strickland *et al.*, 2016).

Research on Fe-N-C catalysts has experienced a surge in recent years due to the increasing need for high-performing and long-lasting catalysts in FCs and MABs. Advancements in synthetic methodologies have resulted in the creation of catalysts that exhibit improved

electrocatalytic activity and stability. Masa *et al*. (2015) investigated the role of transition metals in MNC catalysts through careful synthesis of metal free nitrogen doped carbon and MNC catalysts in which the presence of transition metals was clearly shown to impart significant differences in catalytic activity.

Theoretical and computational modeling have also played a crucial role in advancing the understanding of Fe-N-C catalysts. Density functional theory (DFT) calculations have insights into the electronic structure and catalytic mechanisms, guiding the rational design of more effective catalysts (Tang *et al*., 2024). Moreover, efforts to enhance the practical application of Fe-N-C catalysts have led to their incorporation into various electrochemical devices. For example, recent studies have demonstrated the successful integration of Fe-N-C catalysts into PEMFCs and zinc-air batteries, achieving performance metrics comparable to or even surpassing those of platinum-based catalysts (Tang *et al*., 2024).

2.6.1. Structure of iron nitrogen co-doped carbon catalyst

Iron-nitrogen co-doped carbon catalysts generally comprise of iron coordinated to nitrogen inside a carbon matrix. The predominant arrangement consists of iron coordinated in a pyridinic or pyrrolic configuration, wherein the iron form bonds with nitrogen within the carbon lattice (Jiménez-Ramírez *et al*., 2017). This configuration forms densely packed active sites for ORR) facilitating effective adsorption and reduction of oxygen. The synthesis of Fe-N-C catalysts often entails the thermal decomposition of metal-organic precursors or composites of iron and nitrogen sources supported on carbon (Jiménez-Ramírez *et al*., 2017).

2.6.2. ORR activity of Fe-N-C catalysts

Iron-nitrogen co-doped carbon catalysts demonstrate exceptional ORR performance and selectivity towards the 4e pathway. The selectivity is ascribed to the distinctive active sites created by the iron-nitrogen coordination, which promote the direct conversion of oxygen into water (Strickland *et al*., 2016). The effectiveness of these catalysts is most pronounced in alkaline environments, where the stability and endurance of the carbon matrix are crucial factors in determining catalytic efficiency. Fe-N-C catalysts have demonstrated very promising performance in acidic environments, presenting a viable substitute for platinum-based catalysts in FCs (Gewirth *et al*., 2018; Zhao *et al*., 2019). Incorporating iron into the carbon structure can further boost conductivity, hence further increasing their effectiveness for electrocatalysis of the ORR.

2.6.3. Applications of Fe-N-C catalysts

Fe-N-C catalysts find application in several energy conversion systems, including PEMFCs and alkaline FCs. Their main advantage is their cost-effectiveness, offering a more affordable option compared to precious metals such as Pt. Moreover, Fe-N-C catalysts have promising durability and stability, which are crucial for the sustained operation of fuel cells over extended periods (Osmieri *et al*., 2020; Weiss *et al*., 2020). The versatility and adaptability of the carbon matrix enable the implementation of additional modifications, such as the introduction of heteroatoms or the inclusion of metal nanoparticles (Strelko *et al*., 2000).

2.6.4. Synthesis of Fe-N-C catalysts

Fe-N-C catalysts can be produced using several synthetic procedures that incorporate iron and nitrogen into a carbon matrix as described below.

2.6.4.1. Pyrolysis of metal-organic precursors

A frequently used technique for producing Fe-N-C catalysts involves the thermal decomposition of metal-organic precursors, consisting of carbon, nitrogen, and iron. This approach involves subjecting precursors, such as iron salts (iron chloride), organic polymers, or other nitrogen-rich compounds, to elevated temperatures in an environment devoid of reactive substances. During pyrolysis, the organic molecules breakdown and react with the other entities, resulting in the creation of a carbon matrix that contains iron coordinated to nitrogen, as well as nitrogen functional groups. The products may also contain elemental iron, or iron carbide, depending on the pyrolysis conditions. This synthetic approach provides the ability to regulate the catalyst composition, specifically, the iron-nitrogen coordination and density of Fe-N-C sites by controlling the precursor composition and the pyrolysis conditions.

2.6.4.2. Pyrolysis of metal-organic frameworks (MOFs)

The synthesis of Fe-N-C catalysts often utilise MOFs as a common starting material. MOFs are composed of metal ions that are coordinated to organic ligands, resulting in a distinct porous structure. Pyrolysis leads to decomposition of the organic ligands, while the metal ions create iron-nitrogen coordination complexes inside the carbon matrix (Strelko *et al*., 2000). This technique generates a remarkably porous formation with a substantial surface area, which is advantageous for ORR performance. MOF-derived Fe-N-C catalysts are commonly

produced at elevated temperatures, resulting in partial graphitization and enhanced electrical conductivity (Mehmood *et al*., 2021).

2.6.4.3. Direct impregnation and pyrolysis

Another technique for synthesis of Fe-N-C catalysts involves directly impregnating carbon compounds with iron and nitrogen sources, and then subjecting them to pyrolysis. This method commonly employs carbon supports, such as graphite, activated carbon, or carbon nanotubes, that are infused with iron salts and nitrogen-rich molecules (Zou *et al*., 2019). Subsequently, the mixture is exposed to high temperatures in an oxygen-free environment resulting in the creation of iron-nitrogen coordination within the carbon structure. This technique enables the use of versatile precursor combinations and can generate catalysts with different levels of porosity and graphitization (Xia *et al*., 2011).

2.6.4.4. Sacrificial template method

The sacrificial template method is employed to fabricate distinctive structures in Fe-N-C catalysts by integrating templates that are subsequently eliminated throughout the synthesis process, and post-synthesis treatment. This approach commonly entails including a template material, such as silica or polymer beads, into the carbon precursor, along with iron and nitrogen sources (An *et al*., 2022; Yang *et al*., 2022). The template may be eliminated during thermal treatment process, or through chemical treatment after pyrolysis, resulting in the formation of hollow structures or increased porosity in the catalyst. This method can be employed to produce Fe-N-C catalysts with distinct morphological characteristics, which improves mass transport of substances and thus the turn over frequency of the ORR (Lee *et al*., 2019).

2.6.4.5. Hydrothermal synthesis

Hydrothermal synthesis involves the application of high temperature and pressure in a water-based solution, usually in an autoclave. The conventional approach involves employing a hydrothermal reactor (typically an autoclave) to process precursor materials using iron, nitrogen, and carbon sources (Shen *et al*., 2021). Under the hydrothermal conditions, iron-nitrogen complexes are formed within the carbon matrix, resulting in the creation of a high density of active sites for ORR. Hydrothermal synthesis is commonly employed in tandem with pyrolysis and other techniques to further optimise the structure and properties of the catalyst (He *et al*., 2021).

2.7. Characterization of Fe-N-C catalysts

In-depth characterization of the properties of Fe-N-C catalysts is essential for comprehending their composition, structure, and structure–ORR performance correlation. Various methods are used to analyse the properties of these catalysts, each offering distinct information about their physical and chemical attributes.

2.7.1. Scanning electron microscopy (SEM)

Scanning electron microscopy is a technique that produces micro-to nano-scale images of the surface structure of a catalyst with great resolution. The purpose of using SEM is to visually examine the morphological and surface properties of catalysts , including porosity, graphitic domains, and distribution of iron nanoparticles in Fe-N-C catalysts (Masa *et al*., 2013). This method also enables scientists to determine the shape, identify and quantify cavities, and chemical composition of the constituent elements when coupled with EDS. All these have an influence on the ORR activity (Wiggins-Camacho and Stevenson, 2011).

2.7.2. Transmission electron microscopy (TEM)

Transmission electron microscopy is employed to analyse nano–to- atomic scale structural properties of materials. TEM can detect the existence of iron nanoparticles, determine their size distribution, and examine their association with the carbon matrix (Jin *et al*., 2020; Wang *et al*., 2022). This method is very valuable for examining the arrangement of iron and nitrogen inside the carbon framework, and for determining the crystalline form of the various compositional domains. High-resolution transmission electron microscopy (HRTEM) is capable of detecting lattice fringes, which serve as evidence for the presence of graphitization and other crystalline characteristics.

2.7.3. X-ray diffraction (XRD)

X-ray diffraction (XRD) is employed to ascertain the crystal structure and phase composition of Fe-N-C catalysts. XRD is capable of detecting graphitic domains, amorphous carbon, iron carbide, and other possible crystalline forms present (Jin *et al*., 2020; Park *et al*., 2016; Parvez Ahmad *et al*., 2020). The position of the diffraction peak and their intensity can provide information about the level of graphitization, and the existence of crystalline forms of iron based compounds, such as iron carbide or iron oxides (Jin *et al*., 2020).

2.7.4. X-ray photoelectron spectroscopy (XPS)

X-ray photoelectron spectroscopy is a surface sensitive technique used to analyse the chemical composition of a material and chemical states of the elements present by measuring the energy of emitted electrons resulting from the interaction of X-rays with the material (Jin *et al*., 2020).

XPS is capable of ascertaining the binding energy of different elements, thereby unveiling the specific types of chemical bonds and coordination present in the catalyst (Yang *et al*., 2021). For the Fe-N-C catalyst, this method is especially valuable for determining the oxidation state of iron, nature of the functional groups on carbon, and the specific forms of nitrogen that are present, such as pyridinic, pyrrolic, or graphitic nitrogen, which have a significant impact on the ORR activity. XPS thus offers valuable composition, and structure-performance information of Fe-N-C catalysts, which is valuable for optimization and further catalyst development (Jin *et al*., 2020).

2.7.5. Brunauer-Emmett-Teller (BET)

Brunauer-Emmett-Teller is a surface area analysis method used to measure the surface area of materials. BET surface area analysis quantifies the overall surface area of catalysts, which is directly correlated with their porosity (Jin *et al*., 2020). Nitrogen adsorption is employed in this method to quantify the catalyst's surface area and pore volume. ORR catalysts benefit from having a large surface area and porosity, as these characteristics increase the number of active sites available for the reaction and improve the mass transport of reactants and products. BET analysis facilitates the correlation of the surface properties of the catalyst to the catalytic performance.

2.7.6. Fourier transform infrared spectroscopy (FTIR)

Fourier transform infrared spectroscopy is employed for the purpose of discerning the functional groups and chemical bonds present in a material (Sharma *et al*., 2018). For the Fe-N-C catalysts, FTIR is a valuable tool for identifying the nature of functional groups present, including carbon, oxygen and nitrogen-containing bonds, and other chemical characteristics

that affect the performance of the catalyst (Kumar *et al*., 2019). Additionally, it has the capability to uncover alterations in the chemical composition resulting from thermal treatment and various synthetic procedures.

2.7.7. Electrochemical techniques

The catalytic activity and selectivity of Fe-N-C for the ORR can be assessed using various electrochemical methods. The most common methodologies include cyclic voltammetry, linear sweep voltammetry, and rotating disc electrode voltammetry (He *et al*., 2022). These techniques quantify key performance indicators (KPI) such as onset potential, half-wave potential ($E_{1/2}$), and current density, which offer valuable information on the ORR performance of the catalyst. Electrochemical methods can also ascertain the ORR selectivity, that is, whether the reaction proceeds via the 2-electron or 4-electron pathway. The 4e electron ORR pathway is particularly vital for fuel cell applications to avoid or minimise the formation of hydrogen peroxide which is detrimental to polymer electrolyte membranes (Chlistuno, 2011).

2.8. Assessment of the catalytic efficiency of ORR catalysts

Evaluation of the ORR performance of catalysts entails employing a diverse range of electrochemical techniques and methods to glean insights into activity, stability, and selectivity of the electrocatalysts. The electrochemical approaches that are most commonly used for assessing the efficacy of ORR electrocatalysts are briefly described**.**

Cyclic voltammetry (CV) is a common method employed to assess the electrocatalytic performance of ORR catalysts. The cyclic sweeping of the potential in a CV analysis allows for the assessment of redox processes and catalytic behaviour, as described by Smith *et al*.

(2020). The onset potential for ORR serves as a rough measure of catalytic activity, specifically, regarding the energy efficiency of the reaction. For the ORR, a high positive onset potential indicates a lower energy barrier, and potentially, higher kinetic activity. Cyclic voltammetry (CV) can also reveal the occurrence underlying redox processes in the form of peaks, which may indicate processes on the electrocatalyst as well as the interaction between oxygen and active sites on the catalyst. This technique is beneficial for doing qualitative investigation and initial assessment of catalytic activity.

Linear sweep voltammetry (LSV) is a technique used to measure the current response of an electrochemical system as a function of an applied voltage that increases linearly with time. In LSV, the potential of the working electrode is linearly increased or decreased, yielding data on the current response and other important underlying characteristics (Wang *et al*., 2021). The half-wave potential is an important measure for evaluating the electrocatalytic activity; where higher half-wave potentials indicate better catalytic activity. Linear sweep voltammetry (LSV), under controlled hydrodynamic conditions, for example, using the rotating disc electrode (RDE), can also be employed to determine a number of kinetic parameters of an electrocatalytic reaction.

The RDE is a device used for rotational motion in electrochemical experiments, when the dependence of measured current and potential on controlled mass transport of the reactants to the electrode can be accurately expressed mathematically, enabling to study key kinetic parameters of a reaction. The technique involves the controlled rotation of the electrode at a specific speed, enabling the examination of mass transport and the ORR kinetics (Li *et al*.,

2022). The limiting current under conditions of controlled RDE voltammetry can be described by the Levich equation (2.1).

$$j_L = 0.62nFC_{O2}D_{O2}^{2/3}v^{-1/6}\omega^{1/2} \quad (2.1)$$

where; j_L is the diffusion limited current, n is the number of electrons transferred during the ORR, F is Faraday's Constant, Co_2 solubility of oxygen in the electrolyte solution, D_{O2} is oxygen diffusivity, v is the kinematic viscosity of the electrolyte, and ω is the electrode rotation rate. The number of transferred electrons (n) can be determined from the slope of a plot of j_L against $\omega^{1/2}$.

The Levich plot is a plot of the limiting current versus the square root of the rotation speed. The electron transfer number during the ORR can be determined by RDE studies. This allows for determination of whether the ORR proceeds via the 2-electron or 4-electron pathway (Zhang *et al*., 2021). For both FCs and MABs, it is preferable to have the 4-electron pathway, as it results in the direct conversion of O_2 to water, whereas the 2-electron pathway generates hydrogen peroxide, which is not only detrimental to organic components (e.g. polymer electrolyte membranes), but also has a lower energy efficiency. Some catalysts are affected by hydrogen peroxide which results into catalyst poisoning (Jin *et al*., 2020; Liu *et al*., 2014).

Electrochemical impedance spectroscopy (EIS) is a method employed to assess the charge transfer and resistance characteristics of catalysts. Electrochemical impedance spectroscopy quantifies the catalyst's impedance response at various frequencies, yielding valuable insights into charge transfer resistance and double-layer capacitance (Wang *et al*., 2021). A decrease in charge transfer resistance indicates better electron transfer during the ORR and thus higher possibility for enhanced catalytic activity.

Chronoamperometry is employed to assess the long-term stability and durability of catalysts. This technique involves the application of a consistent potential and monitoring of the current response with time (Wang *et al*., 2021). Chronoamperometry is a valuable technique for evaluating the enduring effectiveness of catalysts in fuel cells and other practical uses (Wang *et al*., 2021).

The typical features of the ORR polarization curve on an ideal catalyst under steady-state hydrodynamic conditions (RDE) is shown in Figure. 2.2. The polarisation curve is a graphical representation of the relationship between current density and applied electrode potential, exhibiting a distinctive "S-shaped" pattern. The LSV curve can be divided into three primary segments, each illustrating an electrocatalytic process characterised by a unique ORR reaction paradigm (Kulkarni *et al*., 2018). More precisely, within the high-potential zone (shown by the green area), the overpotential is insufficient to surpass the reaction barrier and efficiently facilitate the electrochemical process. Consequently, within this range of potential, the kinetics of surface reactions act as a constraining element on the electrocatalytic performance, so creating the zone where surface reactions rule. Within the low-potential zone (pink region), the current remains constant as the overpotential increases. The electrode potential in this location exhibits a substantial deviation from the equilibrium potential. In such circumstances, the reaction rate is sufficiently rapid that the diffusion of oxygen to the surface of the electode through the diffusion layer becomes the limiting factor, while the current remains almost constant as the overpotential increases, leading to the formation of the diffusion-controlled region. The assessment of electrocatalyst activity often relies on the half-wave potential in the mixed controlled region, which is a consequence of the convolution of

surface reactions and mass transport (Zhao *et al*., 2019). The total current in mixed kinetic-diffusion controlled section as described by Koutecky-Levich (K-L) in Figure 2.2, below.

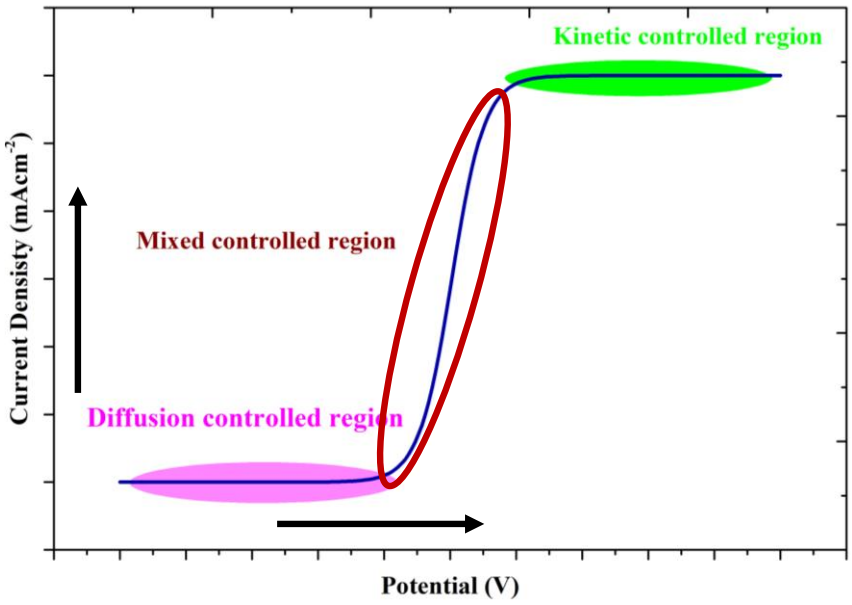

Figure 2.2: Simulation of the ORR polarisation curve on an ideal catalyst under electrode rotation.

2.9. Kinetic parameters for ORR catalytic activity

To gain insight into the ORR performance of the synthesized Fe-N-C catalyst, a number of parameters are required. These parameters can be determined from the electrochemical data obtained from the techniques discussed earlier.

2.9.1. Onset potential and half-wave potential

The onset potential is the potential at which the ORR begins to occur (Batchelor-McAuley, 2022), while the half-wave potential is the potential at which the current reaches half its maximum value. These are critical variables in evaluating ORR catalysts because they provide a measure of catalytic activity (Wang *et al*., 2021). High positive onset potentials and higher positive half-wave potentials generally indicate better catalytic activity.

However, the problem with this measurement can be identified through a simple analysis of the E1/2 as the loading of the RDE catalyst is increased. Consequently, when comparing catalysts based on their half-wave potential, there is a bias towards studies that employ larger loading. Additionally, the dependence on loading further complicates the comparison between studies that utilise different loadings (Wang *et al.*, 2021).

2.9.2. Number of electrons transferred (n)

The ORR can proceed through either a 2-electron or 4-electron pathway, with the latter being more desirable due to its direct production of water without forming hydrogen peroxide. The electrons transfer number during ORR is a crucial variable for assessing catalyst selectivity and efficiency (C. Zhang et al., 2009). Rotating disk electrode (RDE) experiments are commonly used to determine this variable from the polarization data using the Levich equation (2.1).

2.9.3. Tafel slope

The Tafel slope is obtained from a plot of potential or overpotential against the logarithm of the current density based on the Tafel equation (Equation 2.2). The Tafel slope can provide insights into the reaction mechanism, the rate-determining step, and the catalytic activity of ORR catalysts.

$$\eta = \alpha + b\log(j) \quad (2.2)$$

Where η is the overpotential, which is the difference between the electrode potential and the standard equilibrium potential ($\eta = E - E^0$), j denotes the current density, and b is the Tafel slope.

The Tafel slope *b* is an indication of the electrochemical reaction's kinetics and can be derived from the linear portion of the plot of overpotential versus the logarithm of the current density (Shinagawa *et al*., 2015). A lower overpotential suggests that the catalyst is more efficient, requiring less energy to initiate the ORR (Wang *et al*., 2019). This is a critical variable for fuel cell applications, where reducing overpotential can improve energy efficiency and performance.

Tafel slope provides information on the rate-determining step of the ORR and the electron transfer mechanism. A lower Tafel slope generally indicates more efficient catalytic activity, as it suggests that the reaction requires less overpotential to achieve a certain current density (Shinagawa *et al*., 2015). Additionally, the Tafel slope can provide insights into the mechanism by which the catalyst facilitates the ORR.

According to the literature, a slope of approximately 120 $mVdec^{-1}$ suggests that the rate-determining step involves a single-electron transfer, while a slope of around 60 $mVdec^{-1}$ indicates a more complex mechanism with multiple electron transfers (Zhao *et al*., 2021). In addition, the Tafel slope is a measure of the kinetics of an electrocatalytic reaction. In comparative studies, a lower Tafel slope indicates a higher rate of electron transfer, thereby suggesting that the catalyst is more efficient at reducing oxygen.

2.9.4. Exchange current density (j_o)

The exchange current density (j_o) is the current density at which the forward and reverse rates of an electrochemical reaction are equal, resulting in no net current flow. It is typically measured under conditions where the overpotential is zero, providing a measure of the catalyst's intrinsic activity. A high exchange current density indicates a more active catalyst,

suggesting that it can achieve a higher reaction rate at a given overpotential (Conway and Jerkiewicz, 2000).

The exchange current density is an important parameter because it is an intrinsic property of an electrocatalyst that reflects its ability to facilitate electron transfer during the ORR. It is a key parameter for evaluating the effectiveness of a catalyst, as a higher exchange current density indicates a more efficient electron transfer process (Ficca *et al*., 2023).

The Tafel slope and exchange current density are closely related, as both provide insights into the reaction kinetics of the ORR. The Tafel equation can be used to determine the exchange current density by extrapolating the linear portion of the Tafel plot to the zero-overpotential point (Ficca *et al*., 2023). Catalysts with a high exchange current density can achieve comparatively higher current densities at a specific overpotential as opposed to those with low exchange current densities, pointing to superior overall electrocatalytic efficiency.

2.9.5. Charge transfer resistance

Charge transfer resistance reflects the ease with which electrons are transferred between a catalyst and the reactant. A comparatively lower charge transfer resistance indicates more efficient electron transfer and potentially better catalytic activity (Meyer *et al*., 2019). This variable is often evaluated using electrochemical impedance spectroscopy (EIS).

2.9.6. Surface area and active sites

The surface area and density of active sites significantly impact ORR activity. Higher surface area provides more sites for the reaction, while a greater density of active sites leads to improved catalytic performance (Hoshi *et al*., 2013).

2.9.7. Durability and stability

Durability and stability are essential variables for ORR catalysts, especially for long-term applications in fuel cells. Chronoamperometry or chronopotentiometry are among the most commonly used techniques to assess the stability of catalysts (Hoshi *et al*., 2013). The rate of decay in the current response, or increase in potential or overpotential provides insights into the catalyst's resistance to degradation (Vij *et al*., 2016).

CHAPTER THREE

MATERIALS AND METHODS

3.1. Materials and equipment

Natural graphite (LR), Egg albumen (LR), Caffeine (LR), Iron (III) chloride hexahydrate, Nafion solution (5%), Potassium hydroxide (min. assay 85%), isopropyl alcohol 95%, and nitrogen, oxygen gases (min 99% purity).

Vacuum quartz tube furnace (SK-2-2-12 TPA1), Pt wire for the counter electrode (CE), Ag/AgCl in 3M KCl reference electrode (RE), sonicator, Scanning electron microscope (SEM) (ZEISS GeminiSEM 360), and X-Ray Diffractometer (XRD) (Malvern PANalytical, Westborough, MA, USA), a glassy carbon Rotating Disk Electrode (RDE) modified with a film of the catalyst as the working electrode (WE), and Electrochemical analyser (CHI Instruments 710e).

3.2. Methods

3.2.1. Synthesis of Fe-N-C catalyst

The Fe-N-C catalyst was synthesized following a method described by (Huang *et al*., 2019) with slight modification. Nitrogen-doped carbon (NC) was prepared by the pyrolysis of a composite of an egg albumen (0.5089 g) and graphite powder (3.1664 g) respectively. The egg albumen-graphite composite was pyrolyzed in a vacuum oven at 850 °C to produce NC (1.8393 g), cooled and then mixed with 0.0276 g of ferric chloride hexahydrate and pyrolyzed at 850 °C for 2 h under nitrogen gas to obtain iron-nitrogen co-doped carbon catalyst. To remove excess salt and leach away insecurely bound iron species, the produced catalyst

samples were treated with 10 mL of 2M sulphuric acid for 12 hours, followed by washing with excess deionized water. Finally, the catalyst powders were dried overnight in an oven at 70 °C for 12 hours, later weighed (1.7418 g). This procedure was repeated with caffeine as the nitrogen source to give catalyst 2 (2.4023 g). The samples were labelled as OSS_1 and OSS_2, respectively.

3.2.2. Physical chemical characterisation of the catalyst

The X-ray diffraction (XRD) patterns of the catalyst powers were obtained using an X-ray diffractometer (Malvern PANalytical, Westborough, MA, USA) with a Cu Kα radiation source at a voltage of 40 kV and current of 40 mA. SEM images were recorded using a scanning electron microscope (ZEISS GeminiSEM 360) equipped with an Energy-Dispersive X-ray (EDX) spectrometer (Smart EDX).

3.2.3. Electrocatalytic characterisation of the synthesized catalyst

3.0 mg of OSS1 catalyst were dissolved in water (490 µL), isopropyl alcohol (490 µL) and 20 µL of Nafion (5%) followed by ultrasonication for 30 min. 5.3 µL of the resulting catalyst ink was pipetted on a polished glassy carbon (GC) RDE and left to dry in air. All measurements were recorded at room temperature in KOH (0.1M) using an electrochemical analyser (CHE 710E, USA) in a 100 mL volume 3-electrode beaker cell. The electrolyte was first deaerated by bubbling through nitrogen for 10 minutes. Electrode conditioning was carried out by running 20 cyclic voltammograms between 0.2 and -0.8 V (Ag/AgCl in 3M KCl), respectively, at a scan rate of 0.01 V/s to obtain reproducible voltammograms, then a linear sweep voltammogram for background correction was recorded under a nitrogen environment. For ORR measurements, the concentration of oxygen in solution was maintained by purging

high-purity oxygen through a separate fine Polytetrafluoroethylene (PTFE) tubing (0.8 mm). After the purging, the oxygen was lifted above the solution level, and the gas allowed to flow above the solution to maintain oxygen saturation and investigated for the ORR by recording LSV curves at various RDE rotation speeds at room temperature. The measurements were taken with a Ag/AgCl in 3M KCl reference electrode, a platinum coil as counter electrode and catalyst supported on a glassy carbon RDE with a loading of 0.2 mg cm^{-2} as the working electrode. The stability of the catalyst was assessed using chronoamperometric tests, where the current density for the ORR was determined at a constant potential of -0.55 V vs. Ag/AgCl in a 3M KCl solution over a certain time period in a 0.1M KOH electrolyte solution.

3.2.4. Obtained results

The Fe-N-C electrocatalysts are expected to exhibit improved ORR performance compared to the Fe-free, N-free and Fe- and N-free carbon catalysts. The kinetic study provided insight into the mechanism of the ORR on the synthesized Fe-N-C catalysts, while the physical-chemical properties of the catalysts informed structure-performance correlations allowing for optimization of the catalyst synthesis conditions.

3.2.5. Data analysis

3.2.5.1. Characterisation of the synthesized catalyst

SEM high-resolution micrographs were used to analyze the catalyst surface properties, particle size, and distinctive morphological characteristics. EDX maps were used to create composition maps that show the distribution of iron, nitrogen, and carbon within the catalyst. X-ray diffraction (XRD) was used to determine the crystalline structure of the catalysts and probe the presence of specific phases, such as Fe, Fe_3C, iron oxides and graphitic carbon

structures, among others. Additionally, the XRD peaks were used to compute the size of the crystallites using Scherrer equation:

$$\tau = \frac{K\lambda}{\beta cos\theta} \quad 3.1$$

where τ is the mean size of the crystalline particles, *K* is the shape factor (a dimensionless number), λ is the wavelength of the X-rays, β is the light broadening at Full Width at half maximum (FWHM) intensity, and θ is the Bragg angle (Aguilar, 2013).

3.2.5.3. Kinetic analysis of the ORR

3.2.5.3.2. Determination of the kinetic current density (j_k), electron transfer number (n), and reaction rate constant (k) of the ORR

Kinetic analysis of the polarization curve was based on Koutecky–Levich theory which gives the measured current, j, as given by equation 3.2

$$\frac{1}{j} = \frac{1}{jk} + \frac{1}{jl} \quad (3.2)$$

where j_k is kinetic current density and j_l is the diffusion limiting current. The kinetic current is given by,

$$jk = nFkAC_{O2} \quad (3.3)$$

where n is overall number of the electrons exchanged, F is the Faraday's constant (F = 96,487 C/mol), k is reaction rate constant, A is electrode surface area, 0.1256 cm^2 and C_{O2} is the oxygen solubility.

Diffusion limiting current (j_l), which can be directly obtained from the polarization curve, depends on rotation rate and is given by the Levich equation as,

$$j_l = 0.62nFC_{O2}D_{O2}^{2/3}v^{-1/6}\omega^{1/2} \quad (3.4)$$

where F the is Faraday's Constant, C_{O2} solubility of oxygen in electrolyte solution, D_{O2} is the oxygen diffusivity, v is kinematic viscosity of the electrolyte, and ω is the electrode rotation rate. In 0.1M KOH, the solubility of oxygen is 1.2×10^{-6} mol/cm^3, oxygen diffusivity is 1.9×10^{-5}cm^{-2}s^{-1}, while kinematic viscosity of the solution is 0.01 cm^{-2}s^{-1} (Jin *et al*., 2020). From Equations 3.2 and 3.4, a general equation, where the measured current density is expressed as a function of the rotation rate can be written as:

$$\frac{1}{j} = \frac{1}{j_k} + \frac{1}{0.62nFC_{O2}D_{O2}^{2/3}v^{-1/6}\omega^{1/2}} \quad (3.5)$$

This can be simplified as;

$$\frac{1}{j} = \frac{1}{j_k} + \frac{1}{B\omega^{\frac{1}{2}}} \quad (3.6)$$

The inverse of the current density (1/j) was plotted as a function of inverse of the square root of the rotation rate ($\omega^{-1/2}$) to obtain the Koutecky–Levich plots. From the intercept of the plots obtained for various potentials, the kinetic current density was determined by extrapolating the data to zero rotation rate, while from the slope, the overall number of electrons exchanged was calculated as a function of the potential.

3.2.5.3.3. Determination of the Tafel slope, exchange current density (j_o) and charge transfer coefficient (α)

Conventionally, Tafel analysis leads to two important physical parameters, that is: Tafel slope and the exchange current density (j_o). The Tafel relation (Equation 3.7), originally empirically derived, can be theoretically rationalized as follows.

$$\eta = \alpha + blog(j) \quad (3.7)$$

where η is the overpotential, which is the difference between the electrode potential (E) and standard potentials ($\eta = E - E^0$), j denotes current density, and b is Tafel slope. Theoretically, simple electrochemical redox reactions can be described by the Butler-Volmer equation

$$j = j_0\{\exp(-\alpha f \eta) - exp[(1-\alpha) f \eta]\} \quad (3.8)$$

where α is transfer coefficient, f denotes F/RT (F: Faraday's constant, R: the universal gas constant, T: is the absolute temperature), and j_0 is exchange current density. The equation represents the total currents from both reduction and oxidation reactions (opposite signs). First, we consider only the forward (or backward) rates that are significantly larger than the corresponding backward (or forward) reaction rate. From the above equation, the following equation can be derived:

$$\eta = \frac{RT}{\alpha F}\ln(j_0) - \frac{RT}{\alpha F}\ln(j) \quad (3.9)$$

where α as defined in Equation 3.6, thus the intercept obtained from a plot of η vs. log j can be converted into the exchange current density. The Tafel slope gives insight into the reaction kinetics, mechanism and the potential rate limiting step, as well as the exchange current density, which is an intrinsic catalytic parameter (Conway and Jerkiewicz, 2000; Petrii and Tsirlina, 1994). Thus, for analysing electrochemical performance, the Tafel analysis was conjugated with the Butler-Volmer equation as used in many studies (Kulkarni *et al.*, 2018; Shinagawa *et al.*, 2015; Strbac, 2021; Wang *et al.*, 2021a; Zagal *et al.*, 1980; Zhao *et al.*, 2019). All the plots were made using the OriginLab 8.00 data analysis software. The hypotheses were tested using a one-way ANOVA to check if there is a significant difference in the electron transfer number, kinetic current or reaction rate constant for the synthesized catalysts.

CHAPTER FOUR

RESULTS AND DISCUSSIONS

4.1. Results

4.1.1. Synthesis of Iron-Nitrogen Co-doped Catalyst

Two different samples were synthesised from two different nitrogen sources; egg albumen and caffeine (both analytical reagent grades) and the resulting catalysts are hereafter denoted as OSS1 and OSS2, respectively. The schematic view of catalyst synthesis procedure is shown in Figure 4.1, below.

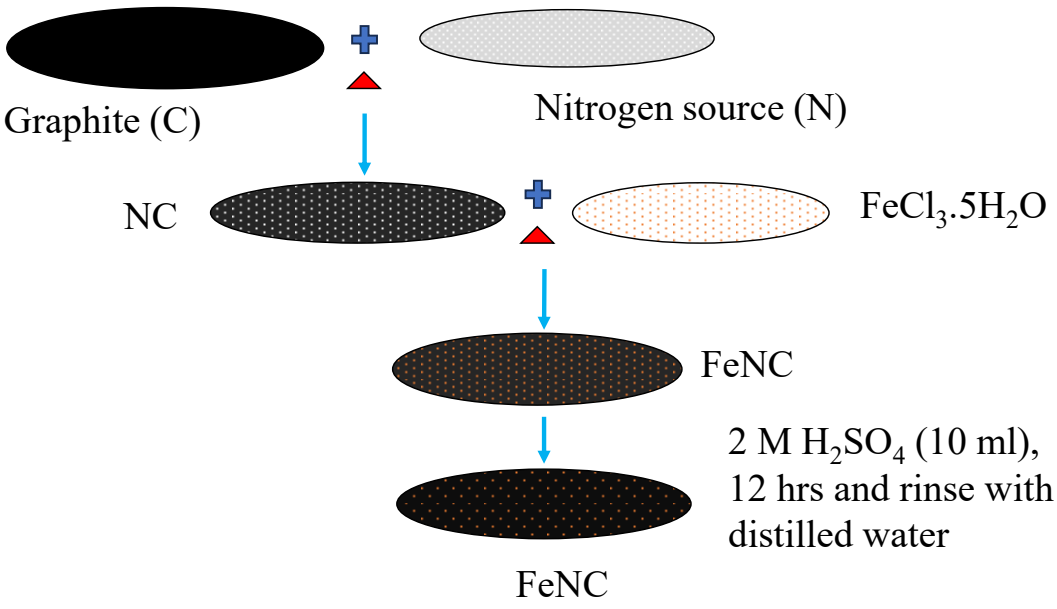

Figure 4.1. Schematic illustration for synthesis of the iron-nitrogen co-doped carbon catalyst (Source: Self design)

4.2.2. Characterisation of the synthesized catalyst

Characterisation of the catalysts was performed by XRD, SEM with integrated elemental analysis by EDX analysis (EDX) (ZEISS DSM 942). Figure 4.2 and 4.3 are SEM micrographs for OSS1 and OSS2, respectively. For both catalysts, the SEM revealed clearly distinct layers of flakes stacked together with evident pores at lower resolution. The flakes were of irregular morphologies with rough porous surfaces. At higher resolution, nanoscale granular structures were observed to be distributed within the catalyst (see Figure 4.2. and 4.3). of the OSS1 and OSS2 catalyst, respectively.

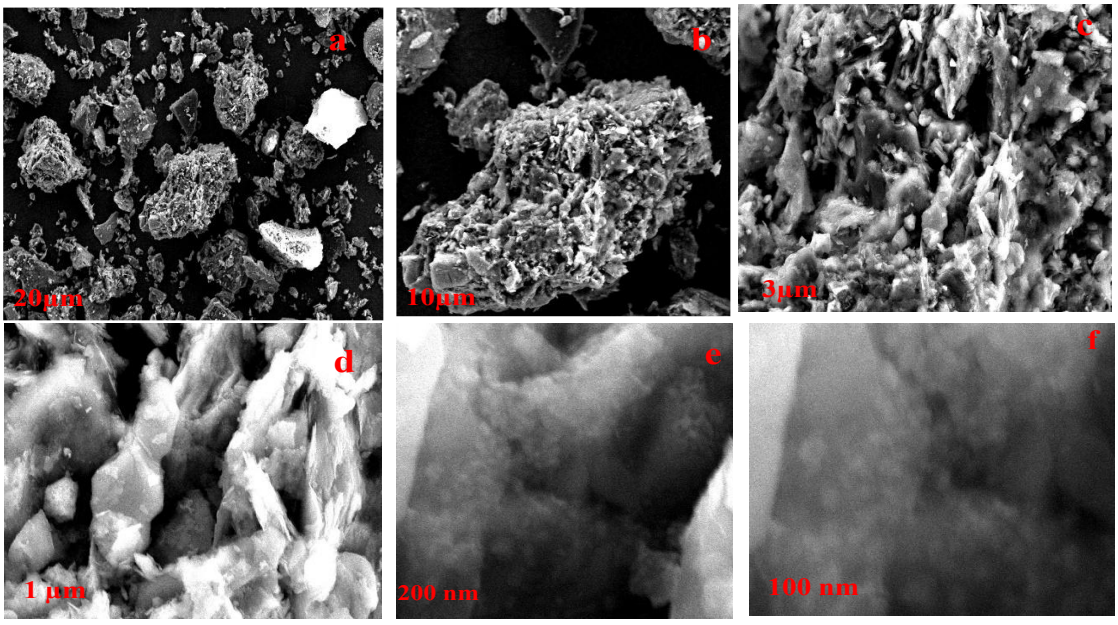

Figure 4.2. Catalyst characterization. (a-f) SEM micrographs at different magnification for the OSS1 catalyst.

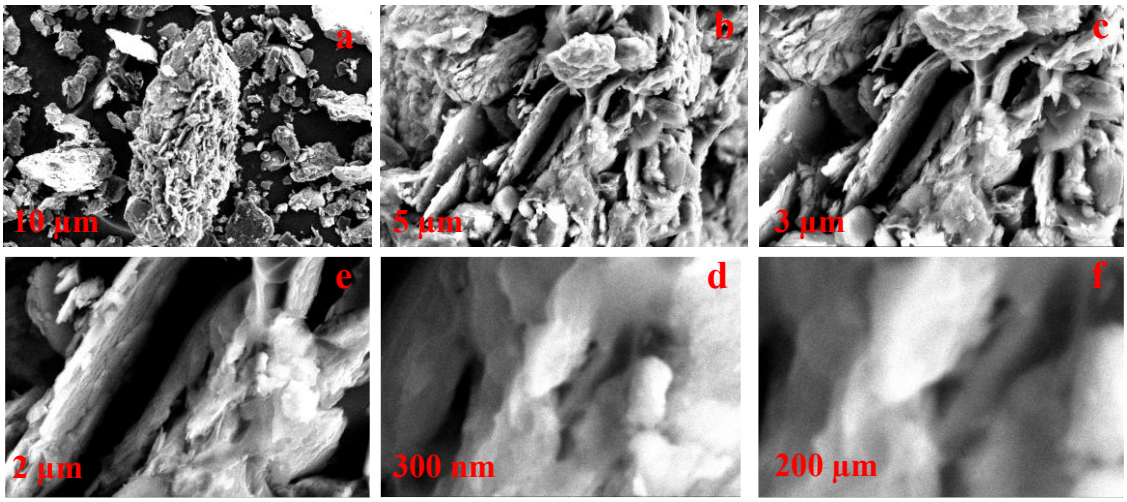

Figure 4.3. Catalyst characterization. (a-f) SEM micrographs at different magnification for the OSS2 catalyst.

Energy dispersive X-ray spectroscopy (EDX) analysis revealed the predominance of carbon as the main element in both catalysts followed by nitrogen and lastly iron, as shown in figure 4.4, 4.5 and figure 4.5, 4.6 for OSS1 and OSS2, respectively. The table 4.1 and 4.2 summarize the elemental composition by atomic weight. EDX analysis also revealed that oxygen as is a major impurity in the samples followed by aluminum. The presence of oxygen on carbon is commonly observed due to surface oxidation of carbon to form various kinds of functional groups, such as carbonyl and hydroxyl species, among others. The origin of aluminum impurities is attributed to contamination of the carbon source.

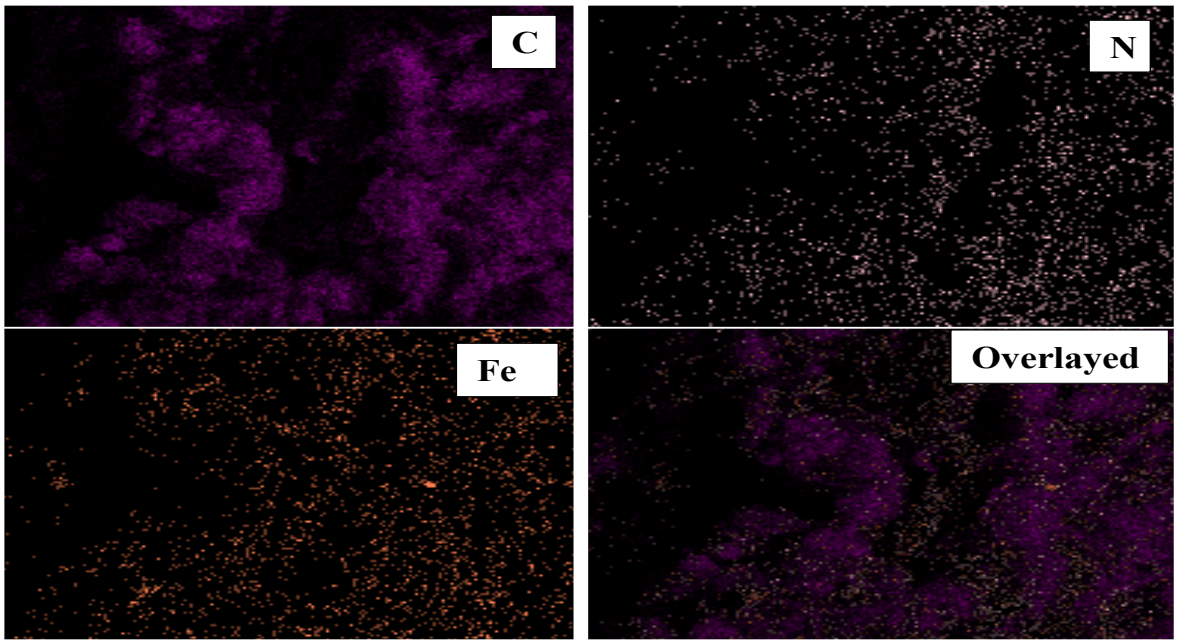

Figure 4.4. Catalyst characterization. EDX elemental-maps showing the distribution of iron, carbon and nitrogen, as well as overlaid C, Fe and N maps in the OSS1 catalyst.

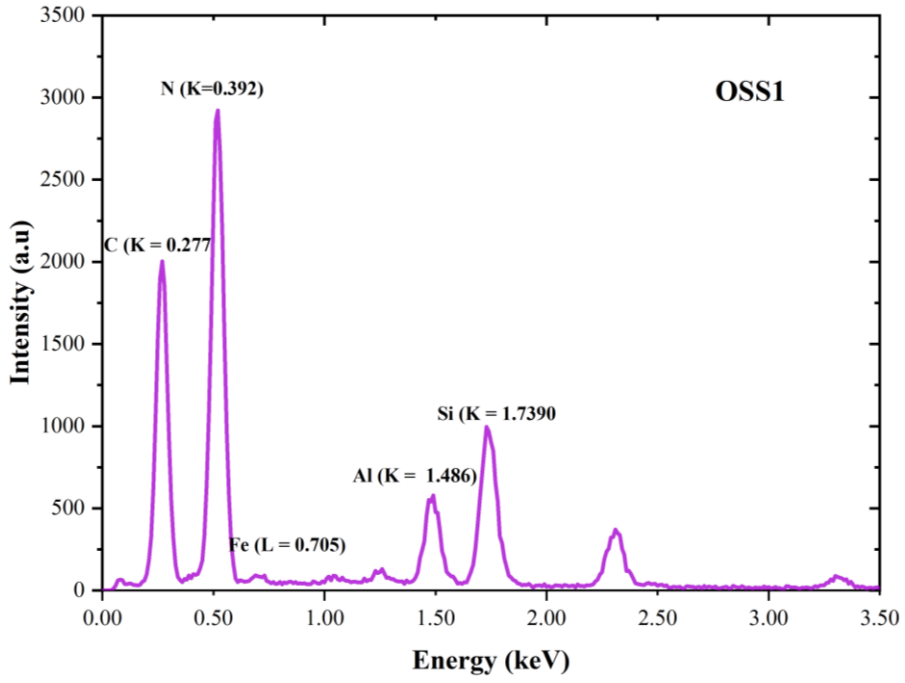

Figure 4.5. EDX spectrum showing the elemental composition of OSS1

Table 4.1 EDS elemental composition of OSS1

Element	Line	Weight%	Atomic%
C	K	53.23	57.74
N	K	1.30	1.28
O	K	47.01	40.56
Fe	L	1.02	0.25

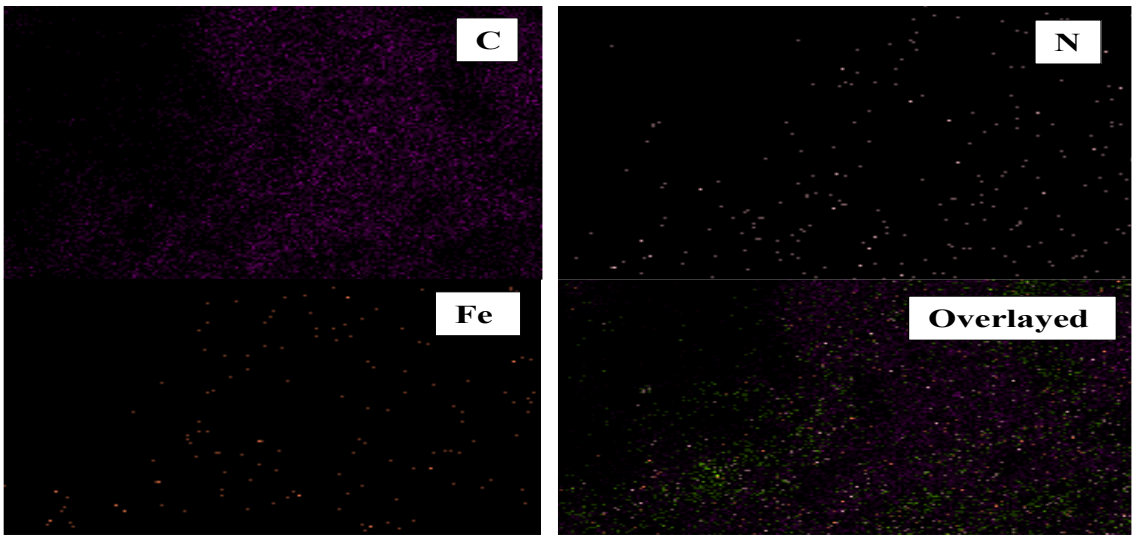

Figure 4.6. Catalyst characterization. EDX elemental-maps showing the distribution of iron, carbon and nitrogen, as well as overlaid C, Fe and N intensity maps in the OSS2 catalyst.

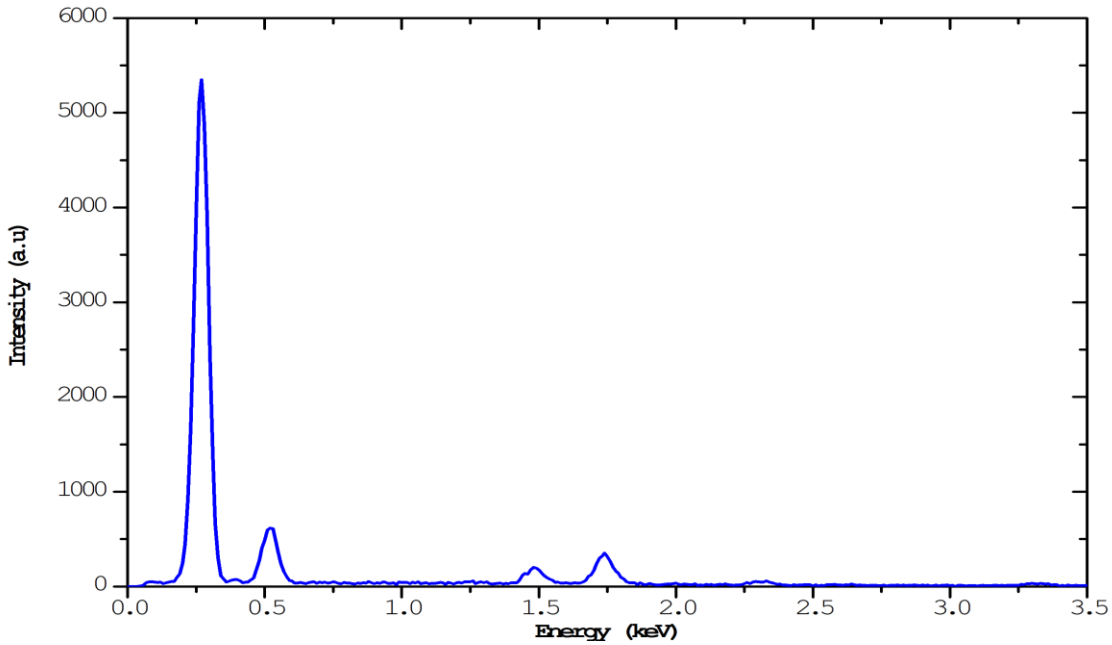

Figure 4.7. EDX spectrum showing the elemental composition of OSS2

The EDS elemental composition analysis as shown in Table 4.2. indicated a carbon-dominant sample with substantial oxygen content and minimal quantities of nitrogen and iron. Carbon (C) is the predominant element, at 59.41 wt% (68.99 at%), suggesting a carbon-rich matrix, potentially graphitic or organic in origin. Oxygen (O) constitutes 27.79 wt% (24.22 at%), indicating potential partial oxidation or the presence of functional groups (e.g., carbonyl, hydroxyl) on the carbon surface.

Nitrogen (N) was detected in trace amounts (1.09 wt% and 1.09 at%), indicating negligible doping or residual nitrogen-containing precursors. Iron (Fe) is present in trace quantities (0.74 wt%, but hardly 0.18 at%), indicating either leftover catalyst particles or inadvertent contamination. The elevated C/O ratio (~2.1 by weight) indicates a somewhat oxidised carbon framework, whilst the nearly similar weight and atomic percentages of nitrogen imply its homogeneous distribution. The little iron content verifies the effective synthesis of a

largely metal-free carbon material, consistent with objectives to reduce dependence on precious metals in catalytic applications.

Table 4.2. EDS elemental composition of OSS2.

Element	Line	Weight %	Atomic %
C	K	59.41	68.99
N	K	1.09	1.09
O	K	27.79	24.22
Fe	L	0.74	0.18

X-ray diffraction (XRD) was used to analyze the crystalline properties of the synthesized Fe-N-C catalysts. The obtained XRD patterns for both OSS1 and OSS2 can be seen in Fig 4.4. Both catalysts exhibited a broad peak at approximately 26.7^0, which corresponds to the (002) crystal plane of graphite carbon (Ilkiv *et al*., 2015). This indicates that the carbon was predominately present in a graphitic form, that is due to the low Fe content in the catalysts which was demonstrated by the characteristic XRD patterns arising from metallic iron, iron carbide, or iron oxide species (Krishnan et al., 2025). The pair of low angle duplet peaks at about $2\theta = 20^o$ are ascribed to species within the graphitic interlayers, likely arising from Fe and nitrogen species embedded with the graphitic layers, as indicated in the SEM micrographs. Small angle X-ray scattering data attribute these duplex peaks to reflections from (2-11) facets of Fe_3N (Chambers *et al*., 2022). The clearly discernible diffraction peak at $2\theta \approx 44.5^o$ is attributed to reflections from the (101) planes of graphitic carbon. The rather weak

diffraction peaks at 2θ ≈ 50° and 54.5° are attributed to reflections from the (024) and (116) planes of α-Fe_2O_3, whose low intensity indicates a very low content of these species.

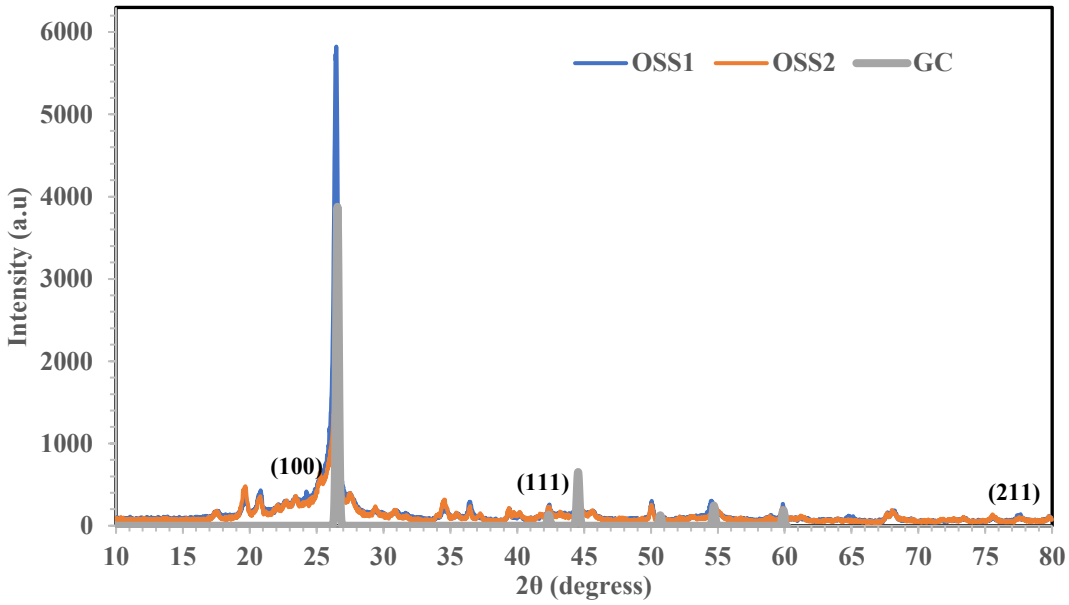

Figure 4.8. X-ray diffraction pattern of the OSS1 and OSS2 catalysts together with the diffraction pattern of graphitic carbon.

The XRD results thus unequivocally revealed the presence graphitic carbon with Fe_3N species embedded within the graphitic interlayers, and a low quantity of crystallites of Fe_2O_3. There was no clear evidence of diffraction patterns attributable to metallic iron. Under conditions of high temperature annealing, carbon has the ability to reduce Fe^{3+} ions, resulting in the formation of Fe nanoparticles. Additionally, some of the Fe^{3+} ions may react with N atoms, leading to the formation of Fe_3N. Fe_2O_3 may be readily produced through the oxidation of metallic Fe due to air exposure (Mi *et al.*, 2020). The crystal sizes of Fe_2O_3 and Fe were not

determined using the Scherer equation because the diffraction peaks are too weak to reliably determine the particle sizes.

4.2.3. Electrochemical tests

All the three catalysts revealed similar patterns with a characteristic first peak at -0.35 V and current intensity of 1.55 $mAcm^{-2}$ for OSS1 and OSS2 while the GC had an irregular peak at -0.65 V and lower current density of 0.6 $mAcm^{-2}$. The pattern later stabilised with same similar however consistent and significantly close peak intensities. OSS1 and OSS2 stabilised at current density of 0.3 $mAcm^{-2}$ at the same potential of -0.35 V. The electrode conditioning polarisation curves are shown in Figure 4.9, below.

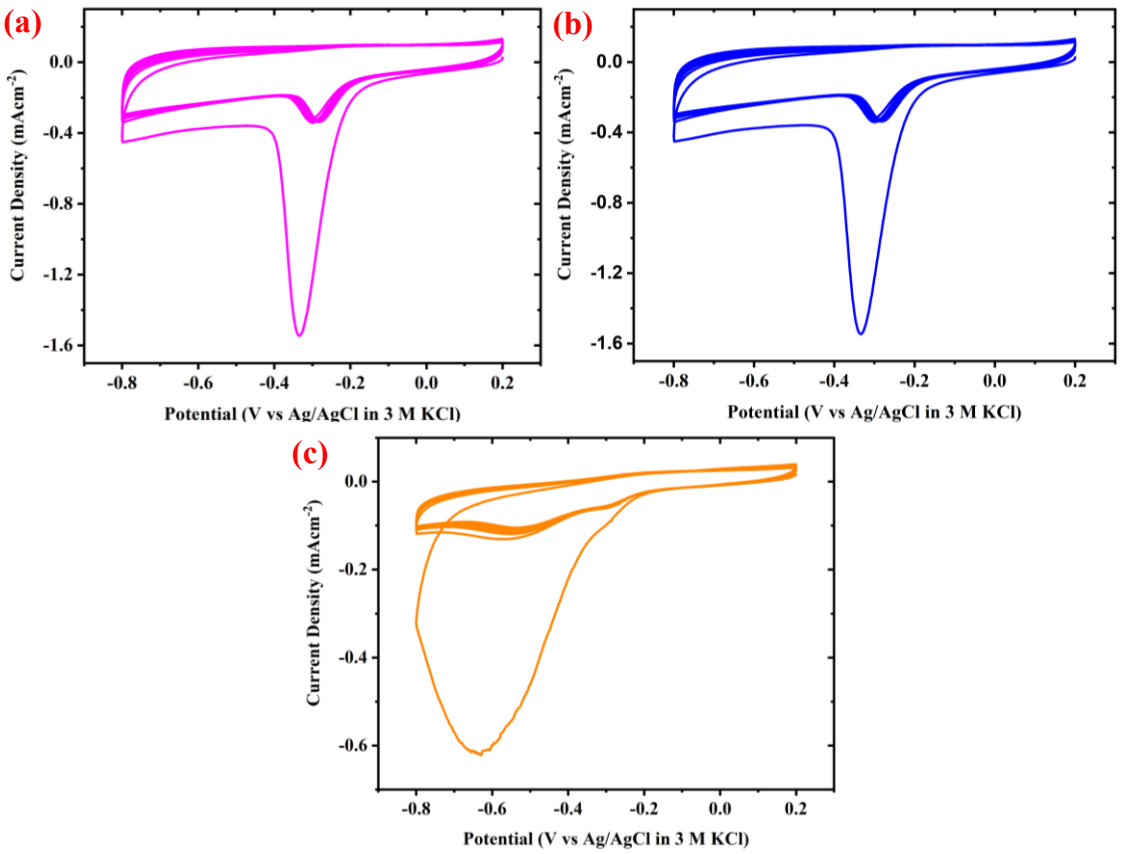

Figure 4.9. Electrode conditioning polarization curves during the ORR on (a) OSS1, (b) OSS2 and (c) GC, in O_2 saturated 0.1M KOH solution at room temperature.

The background reactions in absence of oxygen were investigated for all catalysts. It was found that the background current density increased from GC, OSS1 and OSS2 and shown in Figure 4.9 (a), thus preliminarily, activity of OSS2 was higher than that of OSS1 and GC respectively. This background current was subtracted from the current density of actual ORR tests.

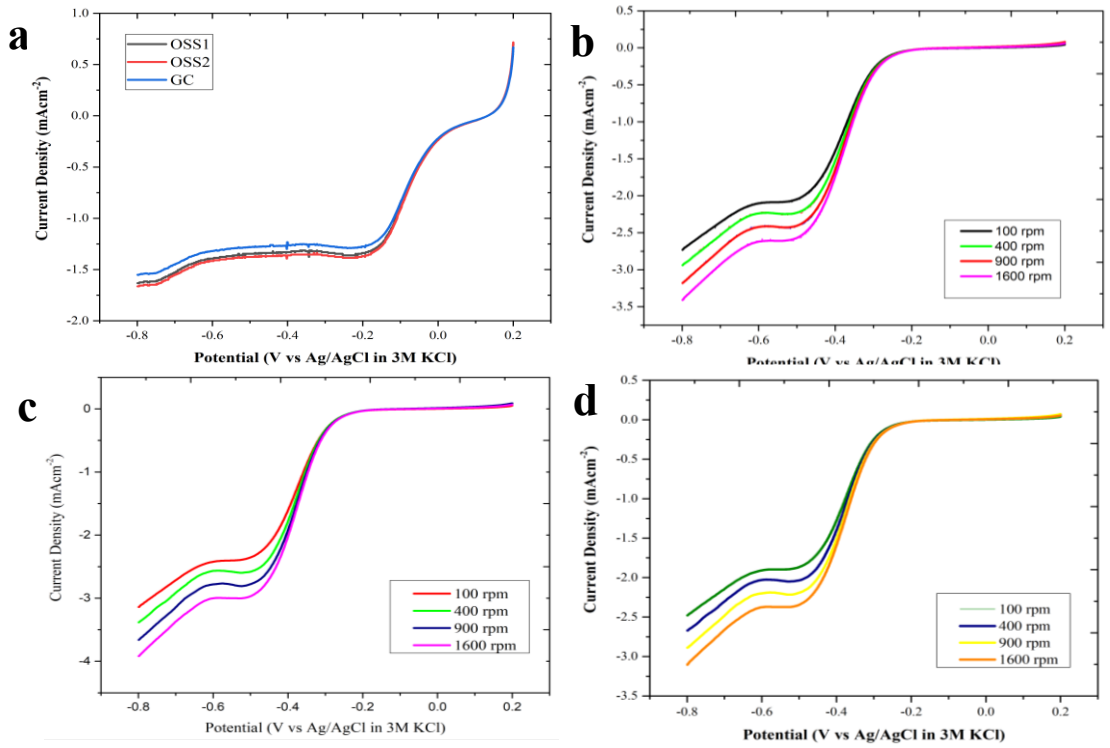

Figure 4.10. Polarization curves during the ORR on (a) Background reactions (b) OSS1, (c) OSS2 and (d) GC, in O_2 saturated 0.1M KOH solution at room temperature.

The electrocatalytic performance of the catalysts during ORR was investigated by linear sweep voltammetry (LSV) tests using RDE in a three-electrode cell in oxygen saturated KOH (0.1M) solution at room temperature. The polarization curves, K-L plots (Figure 4.10 (b-d)) and Tafel slopes (Figure 4.12 (a-c)) of the synthesized OSS1 and OSS2 catalysts, and for bare glassy carbon (GC) as reference are shown in Figure 4.10. The key performance indicators (KPI) determined from Koutecky- Levich analysis of the data is summarized in Table 4.3, below.

Table 4. 2. Summary of ORR catalytic parameters for the OSS1, OSS2 catalysts and GC.

Kinetic Parameter	GC	OSS1	OSS2
E_{onset} (V)	-0.151	-0.142	-0.130
$E_{1/2}$ (V)	-0.551	-0.541	-0.530
n	2.380	2.938	3.238
j_k ($mAcm^{-2}$)	1.007 at -0.290 V	1.609 at -0.423 V	2.189 at -0.466 V
k (s^{-1})	3.621	4.741	5.845
Tafel slope ($mV\,dec^{-1}$)	95.92	103.61	114.65
a ($mA\,cm^{-2}$)	0.354	0.349	0.459
α	0.073	0.073	0.056

The onset potential was -0.151, -0.142 and -0.130 V for glassy carbon, OSS1 and OSS2 respectively. The half wave potential was -0.551, -0.541 and -0.530 V for OSS1, OSS2 and GC, respectively.

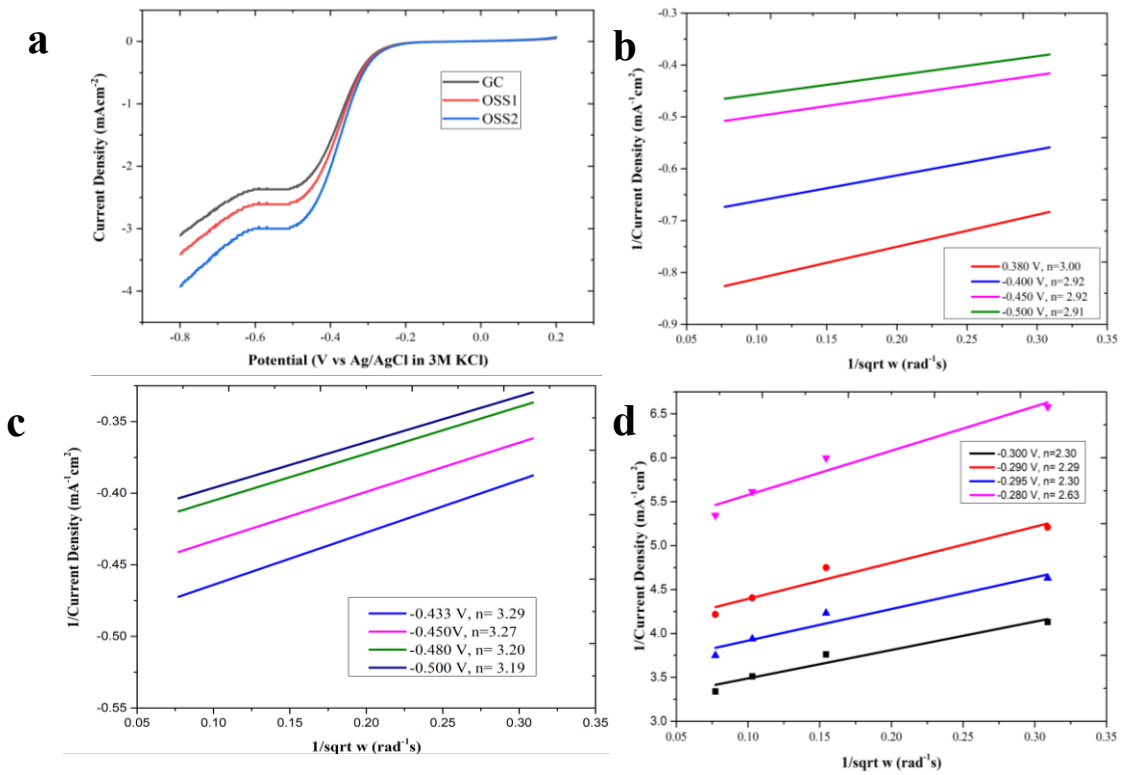

Figure 4.11. The overlayed polarisation curves at 1600 rpm for all the catalysts (a) and Koutecky-Levich plots for (b) OSS1, (c) OSS2 and (d) GC.

The high onset of the ORR on OSS2 compared to the other samples means that OSS2 was able to surmount the ORR energy barrier with comparatively more relative ease than on the other surfaces. This basically indicates that the initial activation of the ORR is kinetically faster on OSS2, however, the onset potential of the ORR alone is insufficient to deduce the overall kinetics of the ORR on the various catalysts. A catalyst with a comparatively higher onset potential doesn't necessarily translate into faster ORR kinetics due to other factors that control the overall reaction kinetics. All the KPIs, including the kinetic current density, Tafel slope, electron transfer number and exchange current density have to be considered in tandem in order to deduce the catalyst with the fastest ORR kinetics.

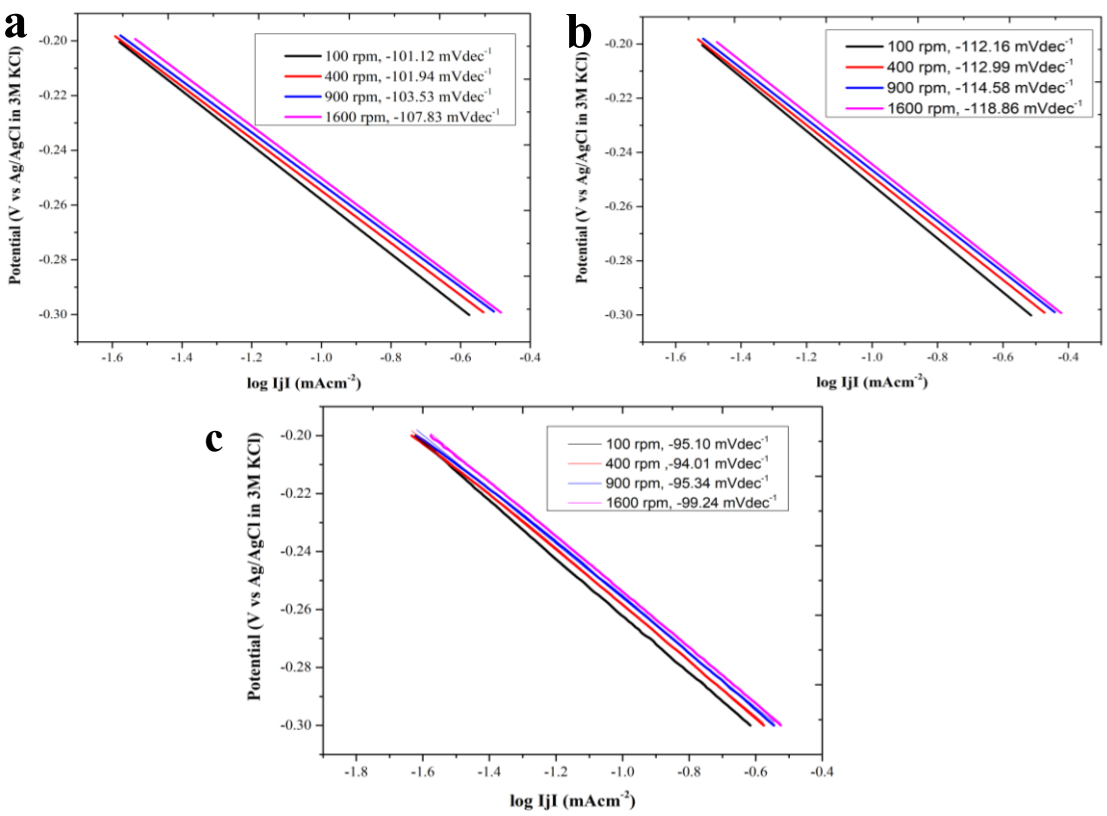

Figure 4.12. Tafel plots for a) OSS1; b), OSS2; and c) GC at various rotation speeds.

The average Tafel slopes for the catalysts recorded was 103.61 and 114.65 for OSS1 and OSS2 respectively and 95.92 for GC as shown in Table 4.3. The individual Tafel slopes for OSS1 ranged from 101.12 to 107.83, 112.16 to 118.86 and 95.10 to 99.24 $mVdec^{-1}$ for OSS1, OSS2 and GC, respectively. The Tafel slope increased with increasing electrode rotation speed.

4.3. Discussions

4.3.1. Characteristics of the iron-nitrogen co-doped catalyst

Scanning electron microscopy (SEM) micrographs revealed an intricate network of interconnected sheets with exposed pores with sizes ranging from micropores to mesopores. The creation of these pores is ascribed to the disintegration of organic precursor materials

during pyrolysis, which liberates gases that generate a porous framework. Iron promotes nucleation and graphitization of carbon resulting in rough surface morphology of the observed carbon sheets (Feng *et al*., 2021). The observed coarse textures or fibrous configurations were also reported by (Chen *et al*., 2018). At elevated temperatures, nitrogen precursors undergo decomposition liberating nitrogen which coordinates the carbon and iron species. The nitrogen can be pyridinic or pyrrolic N doping depending on whether the resultant structure is a 6 or 5 ring structure respectively. The iron and nitrogen centers act as active sites of the catalyst due to higher charge density at these centers. The charge density is attributed to high electronegativity difference between iron and nitrogen with carbon (Jiménez-Ramírez *et al*., 2017)

The SEM micrographs also revealed defects like cracks or voids in the carbon structure, which are frequently associated with stress caused by high temperatures (Singh *et al*., 2020). In addition, introduction of foreign nitrogen atoms can generate defects in carbon structure, hence increasing catalytic activity by offering a greater number of reactive sites (Park and Chen, 2018). There was no irrevocable evidence of the presence of metallic iron particles or clusters neither from the SEM micrographs nor from the XRD data. Metallic particles or clusters can be easily distinguished in SEM images as bright spots because they have a higher atomic number (Johnson and Li, 2017). XRD data revealed interlayer species in the carbon matrix ascribed to Fe_3N. There was evidence of trace amounts of Fe_2O_3 in the samples from the XRD patterns. Metallic iron particles can be created from iron precursors during pyrolysis due the reductive conditions. When exposed to air, they readily undergo transformation into oxide forms.

The presence of nitrogen in SEM may not be directly visible, but it is not expected to greatly impact the morphological properties of the sample. Nitrogen doping induces structural defects in the carbon matrix and modifies its electrical characteristics. These modifications impact the properties, fostering the formation of distinct surface structures as reported by (Li *et al.*, 2021).

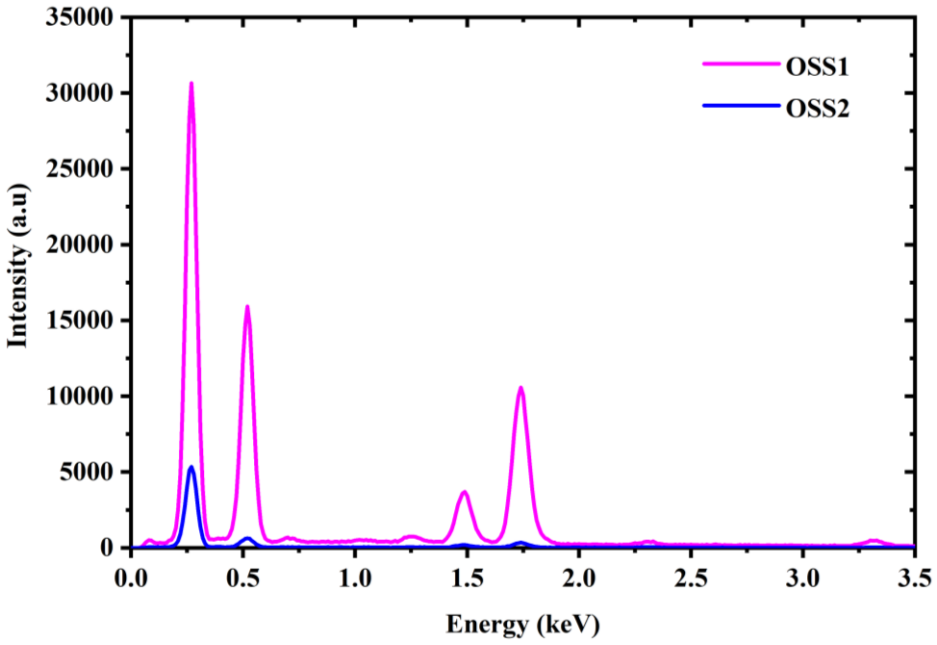

Figure 4.13. EDS spectra of the OSS1 and OSS2 catalysts showing variation of the intensity against energy of the emitted X-rays.

Energy-dispersive X-ray spectroscopy (EDX) provided valuable information about the elemental composition and distribution of the constituent elements C, Fe and N in the Fe-N-C catalysts. The presence of the iron (Fe) peak (L=0.705), nitrogen (K=0.392), and carbon peak (0.277), as verified by the EDS reference sheet, indicates the effective synthesis of the iron-nitrogen co-doped catalyst. The carbon intensities in both catalysts surpassed those of

nitrogen and iron, hence confirming a larger composition of carbon in both samples, as expected. The catalytic activity of the Fe-N-C catalysts depends on the co-existence of an appropriate quantity of both iron and nitrogen in a specific configuration (Feng *et al*., 2013; Liang *et al*., 2014; Osikoya *et al*., 2015; Park *et al*., 2016; Wei *et al*., 2015; Wiggins-Camacho and Stevenson, 2011; Zhao *et al*., 2013).

4.3.2. ORR activity of the synthesized Fe-N-C catalysts

4.3.2.2. Koutecky-Levich analysis

The kinetic current density values for glassy carbon, OSS1, and OSS2 were 1.0073, 1.6087, and 2.1889 $mAcm^{-2}$ at -0.423, -0.466 and -0.290 V respectively. The overall electron transfer number was 2.38, 2.94, and 3.24, while the reaction rate constant was 3.621, 44.741, and 5.845 s^{-1}, respectively. Out of all the catalysts, OSS2 had the highest electron transfer number (3.24), signifying that ORR primarily followed the four-electron pathway. The electron transfer number of OSS1 was 2.94, indicating that both the four-electron pathway and the two-electron transfer pathways occur in parallel, but with a little higher tendency towards the production of hydrogen peroxide. GC had the lowest electrons transfer number of 2.38, suggesting a higher propensity for hydrogen peroxide formation (Zhou *et al*., 2020). The Koutecky-Levich analysis data is summarized in the bar graph in Figure 4.14.

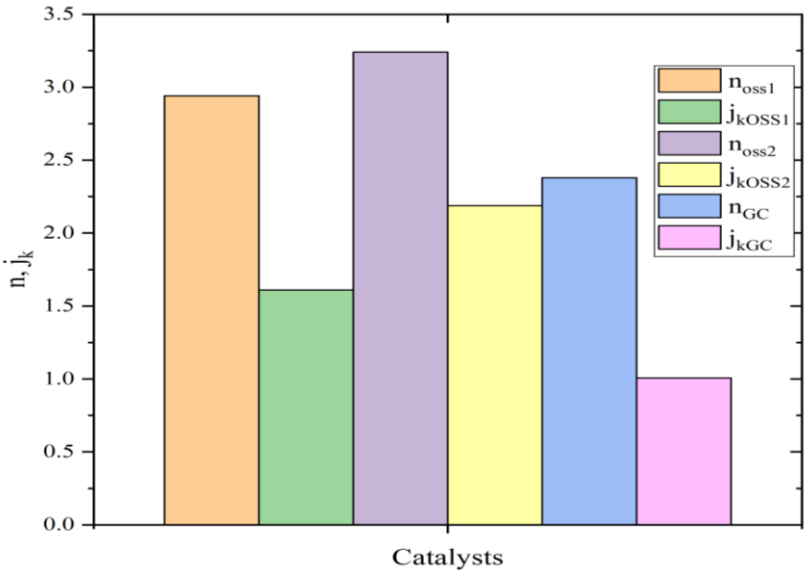

Figure 4.14. Bar graphs showing number of transferred electrons (n) and kinetic current (j_k) of the ORR on OSS1, OSS2 and on GC.

4.3.2.3. Comparison of the electron transfer number (n) for the catalysts.

The electron transfer number during the ORR is a key metric indicating the pathway through which the reaction proceeds. A value of 4 signifies a direct reduction of oxygen to water, while a value of 2 suggests formation of hydrogen peroxide as an intermediate. Combining these insights, OSS2 emerged as the best-performing catalyst due to its high of electron transfer number, the highest kinetic current, and the fastest reaction rate constant. This indicates that OSS2 has the highest efficiency making it the most suitable for applications requiring efficient 4e- oxygen reduction to water with none or minimal production of hydrogen peroxide. OSS1 also performed well but was slightly less efficient than OSS2. GC showed the least efficient characteristics, with a much lower electron transfer number, lower kinetic current, and much lower reaction rate constant.

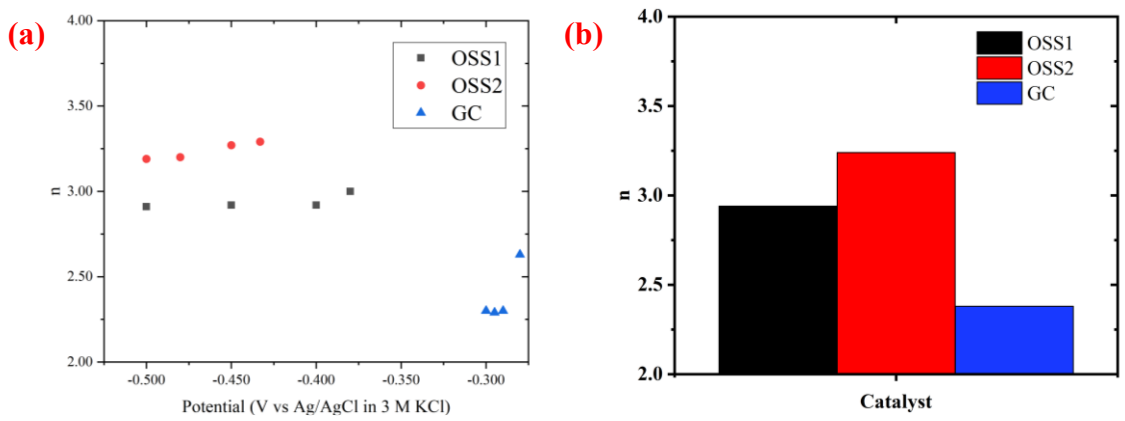

Figure 4.15. Comparison of electron transfer number (n) of synthesized catalysts, OSS1 and OSS2 and that of GC at -0.423, -0.466 and -0.290 V.

(a) Plot of electron transfer number against the applied potential. (b) Bar graph showing average electron transfer number for each catalyst and their relationship to the 2 or 4 electron transfer number.

4.3.2.4. Dependence of elctron transfer number on applied potential

As clearly illustrated in Figure 4.14, all the studied catalysts revealed a linear a relationship between applied potential and *n* during ORR on both the OSS1 and OSS2 catalysts, as well as on GC. The number of electrons transferred increases with increasing overpotential. This relationship is consistent with results reported in the literature (Shen *et al*., 2019). At higher overpotentials, the number of electrons transferred is higher, suggesting a predominance of the four-electron pathway, which leads to the direct conversion of oxygen to water. At lower overpotentials, the number of electrons transferred gradually decreases, indicating a shift towards the 2e pathway, which involves the formation of H_2O_2 as an intermediate. This trend, where *n* decreased from 3.00 at -0.380 V to 2.91 at -0.500 V, points to a transition in the ORR

mechanism, with the 4e- being favoured at high overpotentials while low overpotentials favoured the 2e- pathway, implying more generation of H_2O_2.

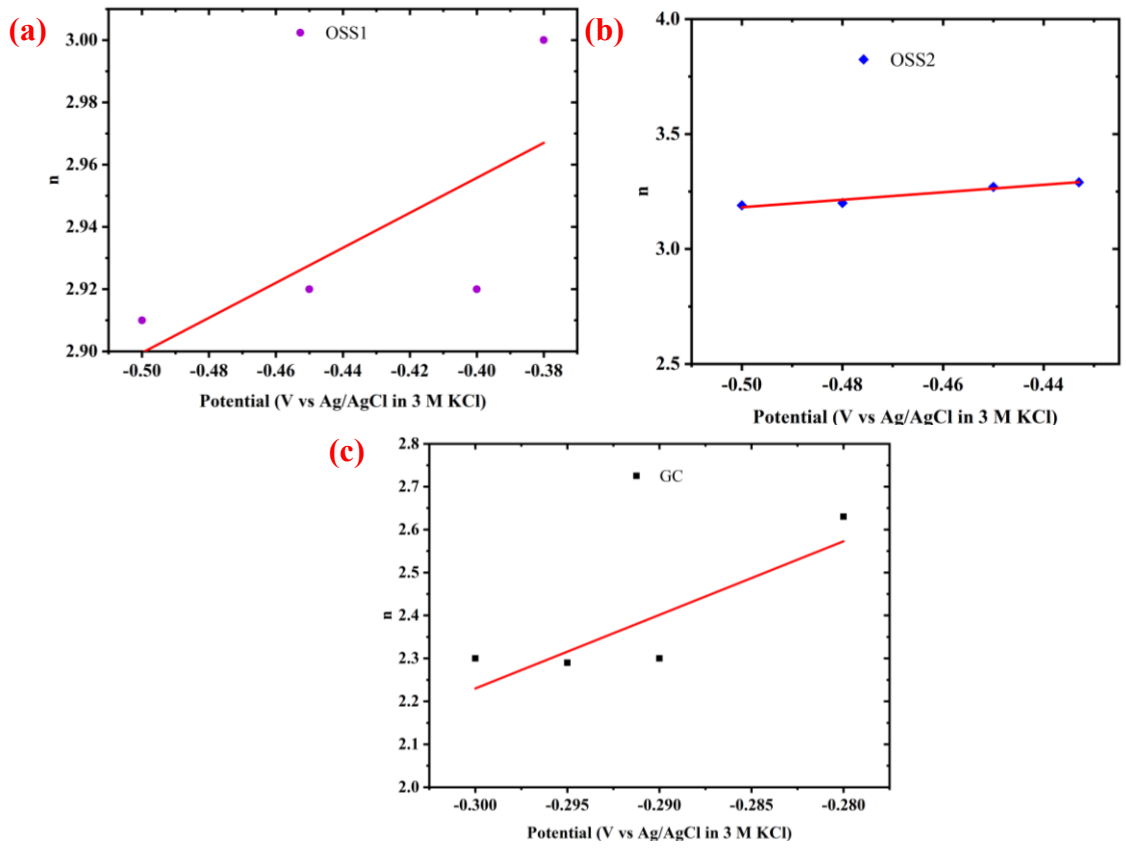

Figure 4.15. Variation of the number of electrons transferred against the applied electrode potential for OSS1, OSS2, and GC, respectively.

4.3.2.5. ORR reaction mechanism on the OSS1 and OSS2 catalysts.

Tafel plots for the ORR on the three catalysts, namely GC, OSS1, and OSS2, offered valuable insights into the ORR reaction mechanism on the catalysts. GC had a Tafel slope of 95.92 mV/decade, indicating an intricate process controlled by both electron transport and subsequent chemical reactions. Platinum catalysts are known to successfully facilitate the 4-electron reduction pathway in alkaline environments, and this mixed control mechanism is a

feature of such catalysts (Antolini, 2009). The findings for the OSS1 catalyst, which had a Tafel slope of 103.61 mV/decade, is not significantly different from that of GC meaning that the ORR on OSS1 follows a similar pathway as on GC. However, the activation barrier for either the electron transfer step or a later chemical step is higher. The OSS2 catalyst, was characterized by a Tafel slope of 114.64 mV/decade, suggesting that a chemical step is the controlling factor in the reaction mechanism. This could be attributed to variations in surface characteristics or active site configurations compared to OSS1. The observed differences in Tafel slopes emphasized the impact of catalyst composition and structure on the ORR mechanism. From the Tafel slopes above, the following ORR mechanisms have been proposed for each catalyst as summarized in Table 4.4, below.

Table 4.4. ORR mechanism for the synthesized catalysts.

Catalyst	Tafel slope ($mV dec^{-1}$)	ORR mechanism
OSS1	103.61	$O_2 + e \rightarrow O_2^-$ (RDS) $O_2^- + H_2O + e \rightarrow HO_2^- + OH^-$ $HO_2^- + H_2O + 2e \rightarrow 3OH^-$
OSS2	114.65	$O_2 + e \rightarrow O_2^-$ $O_2^- + H_2O + e \rightarrow HO_2^- + OH^-$ (RDS) $HO_2^- + H_2O + 2e \rightarrow 3OH^-$
GC	96.92	$O_2 + 2H_2O + 4e \rightarrow 4OH^-$

The ORR occurs by one of two possible major pathways depending on the final product, that is hydrogen peroxide or water. In addition, there are several factors that influence the ORR mechanism, including the mode of adsorption of oxygen, chemical composition and physical characteristics of the catalyst (Van Ede and Angst, 2023). Oxygen may approach a single active site either side-ways or end-on. At a dual site, the side-ways approach leads to

adsorption of O_2 on two active sites simultaneously forming a bridge-cis bond. Depending on the proximity of dual sites, the end-on approach to a dual site may lead to O_2 binding in a bride-trans configuration. On well-defined structures, such as monocrystalline surfaces, the mode of O_2 adsorption is easy to predict since the inter-atomic distances in two-dimensional space are known. After the adsorption step, the subsequent multi-step proton-coupled electron transfer steps, and chemical steps, determine the value of Tafel slope, depending on the rate-determining elementary reaction. If the first electron transfer step is rate limiting, the theoretical value of the Tafel slope would be around 59 mv/decade. Conversely, if a chemical step is rate determining, the theoretical value of the Tafel slope would be close to 118 $mVdec^{-1}$.

From the Tafel slope data in Table 4.5, it can be concluded that GC exhibited a mixed mechanism that is characterized by a combination of factors, without a specific single step dominating the mechanism and the reaction rate. Similarly, OSS1 also exhibited a mixed control mechanism, but with indication of a charge transfer step being rate limiting. On the other hand, it is very evident that OSS2 had a chemical step involving the intermediate species that determines the rate.

The observed Tafel slopes for these catalysts are consistent with the results reported by other researchers. For example, catalysts based on Pt in alkaline solutions usually exhibit Tafel slopes that vary between 60 and 120 mV/decade. The particular values depend on how the catalyst is prepared and the conditions of the experiment. This range indicates the prevalence of mechanisms that involve both electron transport and chemical steps (Antolini, 2009). Iron-nitrogen co-doped carbon catalysts have been found to exhibit Tafel slopes ranging from 80 to 120 mV/decade, suggesting a variety of processes and factors at the active sites. According to

Liu *et al.* (2011), they discovered that Fe-N-C catalysts exhibit Tafel slopes ranging from 90 to 110 mV/decade, which aligns with the values recorded for OSS1 and OSS2 in this study. The similarities indicate that the oxygen reduction reaction on OSS1 and OSS2 is controlled by both electron transfer and subsequent chemical reactions, however, with a chemical step being clearly the dominant rate limiting in the case of OSS2 compared to the case in OSS1. The individual Tafel slopes reflect the variations in activation energies and surface features. The alignment of these findings with existing literature validates the deduced ORR mechanisms in these catalysts and emphasizes the influence of catalyst design on electrochemical performance.

CHAPTER FIVE: CONCLUSIONS AND RECOMMENDATIONS

5.1. Conclusions

Iron-nitrogen co-doped carbon catalysts were successfully prepared by the pyrolysis at 850 °C of a mixture of graphite and iron chloride as the carbon and iron sources, respectively, and two different nitrogen sources were studied, that is; egg albumen and caffeine. The ORR activity of the synthesized catalysts in the form of films adsorbed on a glassy carbon rotating disc electrode (RDE) was determined and compared with that of a bare glassy carbon (GC) electrode. The OSS2 catalyst, in which caffeine was used as the nitrogen source emerged the best ORR catalyst in terms of electron transfer number (3.34), kinetic current density (2.19 mA cm^{-2} at -0.466 V) and reaction rate constant (5.85 s^{-1} also at -0.466 V). By contrast, the corresponding values of n, j_k and k for OSS1 were: 2.94, 1.61 mA cm^{-2}, 4.74 s^{-1}, at -0.433 V respectively. On the other hand, the electron transfer coefficient of OSS2 (0.056) was lower than that of OSS1 (0.073), and its Tafel slope (114.65 mV dec^{-1}) was also lower than that of OSS1 (103.61 mV dec^{-1}), however, the difference was not significantly large thus suggesting that the ORR mechanism was similar on the two catalysts. The incorporation of iron and nitrogen into carbon therefore improved the ORR activity of carbon as expected.

5.2. Recommendations

i. Utilizing caffeine as a nitrogen precursor for the synthesis of Iron-Nitrogen co-doped Carbon (Fe-N-C) catalysts by the pyrolysis of a composite mixture of caffeine and $FeCl_3.5H_2O$ (Fe source) dispersed on graphite powder (carbon source), is evidently very promising. Future efforts should focus on further optimizing the amount of egg

albumen and caffeine of the synthesis parameters to enhance the ORR performance. Utilizing caffeine as a precursor presents various benefits, such as cost-effectiveness and sustainability, among others.

ii. Future studies may also investigate the ORR catalytic activity in acidic conditions, as well as its role in hydrogen and oxygen evolution reactions. Assessing the ORR catalytic activity of the synthesized catalysts in acidic electrolytes is essential due to the potential for practical applications, such as in proton exchange membrane fuel cells (PEMFCs).

iii. Additional characterization of the synthesized catalysts using TEM and XPS, among others, to thoroughly elucidate the properties of the catalyst is necessary. TEM and XPS are advanced methods used to analyse the surface structure and chemical composition of materials at the nanoscale. TEM can reveal structural characteristics of the catalysts, including particle size, shape, and distribution. These parameters play a crucial role in determining catalytic activity. XPS examination provides comprehensive insights into the chemical composition and electronic properties of the elements present in the catalysts. Through the utilisation of TEM and XPS, more profound understanding of the catalysts' structural and chemical attributes may be deciphered. This enables the refinement of synthesis techniques and the improvement of their catalytic efficiency.

REFERENCES

Abbo, H. S., Gupta, K. C., Khaligh, N. G., & Titinchi, S. J. J. (2021). Carbon Nanomaterials for Wastewater Treatment. *ChemBioEng Reviews*, *8*(5), 463–489. https://doi.org/10.1002/cben.202100003

Aguilar, Z. P. (2013). Types of Nanomaterials and Corresponding Methods of Synthesis. In *Nanomaterials for Medical Applications*. https://doi.org/10.1016/b978-0-12-385089-8.00002-9

Alam, S. N., Sharma, N., & Kumar, L. (2017). Synthesis of Graphene Oxide (GO) by Modified Hummers Method and Its Thermal Reduction to Obtain Reduced Graphene Oxide (rGO)*. *Graphene*, *06*(01), 1–18. https://doi.org/10.4236/graphene.2017.61001

Alom, J., Hasan, M. S., Asaduzaman, M., Alam, M. T., Belhaj, D., Selvaraj, R., Hossain, M. A., Zargar, M., & Ahmed, M. B. (2023). Catalytical Performance of Heteroatom Doped and Undoped Carbon-Based Materials. *Catalysts*, *13*(5). https://doi.org/10.3390/catal13050823

Alonso-Vante, N., Feng, Y., & Yang, H. (2019). Novel non-precious metal electrocatalysts for oxygen electrode reactions. *Catalysts*, *9*(9), 15–17. https://doi.org/10.3390/catal9090731

Amani, M., Kazemeini, M., Hamedanian, M., Pahlavanzadeh, H., & Gharibi, H. (2015). Investigation of methanol oxidation on a highly active and stable Pt-Sn electrocatalyst supported on carbon-polyaniline composite for application in a passive direct methanol

fuel cell. *Materials Research Bulletin*, *68*, 166–178. https://doi.org/10.1016/j.materresbull.2015.02.053

An, H., Min, K., Lee, Y., Na, R., Shim, S. E., & Baeck, S.-H. (2022). Sacrificial template induced Fe-, N-, and S-tridoped hollow carbon sphere as a highly efficient electrocatalyst for oxygen reduction reaction. *Molecular Catalysis*, *530*, 112589. https://doi.org/https://doi.org/10.1016/j.mcat.2022.112589

Appel, A. M., & Helm, M. L. (2014). Determining the overpotential for a molecular electrocatalyst. *ACS Catalysis*, *4*(2), 630–633. https://doi.org/10.1021/cs401013v

Batchelor-McAuley, C. (2022). Defining the Onset Potential. *Current Opinion in Electrochemistry*, *37*, 101176. https://doi.org/10.1016/j.coelec.2022.101176

Byeon, A., Choi, J. W., Lee, H. W., Yun, W. C., Zhang, W., Hwang, C.-K., Lee, S. Y., Han, S. S., Kim, J. M., & Lee, J. W. (2023). CO2-derived edge-boron-doped hierarchical porous carbon catalysts for highly effective electrochemical H2O2 production. *Applied Catalysis B: Environmental*, *329*, 122557. https://doi.org/https://doi.org/10.1016/j.apcatb.2023.122557

Cells, T. F., Cell, F., Office, T., Cells, F., Office, T., & Cells, T. F. (2016). *3.4 Fuel Cells*. *2015*, 1–58.

Chadly, A., Azar, E., Maalouf, M., & Mayyas, A. (2022). Techno-economic analysis of energy storage systems using reversible fuel cells and rechargeable batteries in green buildings. *Energy*, *247*(February), 123466.

https://doi.org/10.1016/j.energy.2022.123466

Chambers, M. S., Hunter, R. D., Hollamby, M. J., Pauw, B. R., Smith, A. J., Snow, T., Danks, A. E., & Schnepp, Z. (2022). *In Situ and Ex Situ X-ray Diffraction and Small-Angle X-ray Scattering Investigations of the Sol − Gel Synthesis of Fe 3 N and Fe 3 C*. https://doi.org/10.1021/acs.inorgchem.1c03442

Chen, Y., Zhang, X., Wang, A., Zhang, Q., Huang, H., & Feng, J. (2019). *Ultrafine Fe 3 C nanoparticles embedded in N-doped graphitic carbon sheets for simultaneous determination of ascorbic acid , dopamine , uric acid and xanthine*.

Chen, Z., Pei, S., Sun, Y., Xiong, X., Zhang, W., Han, Z., Xu, K., Zhou, Z., Zhang, Y., Feng, W., Wang, L., & Zou, Y. C. (2021). Iron and Nitrogen Co-doped Carbon Spheres as High Efficiency Oxygen Reduction Catalyst. *International Journal of Electrochemical Science*, *16*, 1–15. https://doi.org/10.20964/2021.05.36

Chiralt, A., González-Martínez, C., Vargas, M., & Atarés, L. (2017). Edible films and coatings from proteins. In *Proteins in Food Processing, Second Edition*. Elsevier Ltd. https://doi.org/10.1016/B978-0-08-100722-8.00019-X

Chlistuno, J. (2011). *RRDE and Voltammetric Study of ORR on Pyrolyzed Fe / Polyaniline Catalyst . On the Origins of Variable Tafel Slopes*. 6496–6507.

Conway, B. E., & Jerkiewicz, G. (2000). Relation of energies and coverages of underpotential and overpotential deposited H at Pt and other metals to the `volcano curve' for cathodic H2 evolution kinetics. *Electrochimica Acta*, *45*(25–26), 4075–4083.

https://doi.org/10.1016/S0013-4686(00)00523-5

Debe, M. K. (2012). Electrocatalyst approaches and challenges for automotive fuel cells. *Nature*, *486*(7401), 43–51. https://doi.org/10.1038/nature11115

Dincer, I. (2007). Principles of fuel cells, Xianguo Li, Taylor & Francis, New York, 2006, No. of pages: 572. *International Journal of Energy Research*, *31*(10), 999–999. https://doi.org/10.1002/er.1274

Dou, S., Li, X., & Wang, X. (2020). Rational Design of Metal-Organic Frameworks towards Efficient Electrocatalysis. *ACS Materials Letters*, *2*(9), 1251–1267. https://doi.org/10.1021/acsmaterialslett.0c00229

Duan, X., Ren, D., Wang, S., Zhang, M., Sun, Y., Sun, S., Huo, Z., & Zhang, N. (2023). Carbon materials in electrocatalytic oxidation systems for the treatment of organic pollutants in wastewater : A review. *Carbon Resources Conversion*, *6*(4), 262–273. https://doi.org/10.1016/j.crcon.2023.03.006

Fazio, G., Ferrighi, L., & Di Valentin, C. (2014). Boron-doped graphene as active electrocatalyst for oxygen reduction reaction at a fuel-cell cathode. *Journal of Catalysis*, *318*, 203–210. https://doi.org/10.1016/j.jcat.2014.07.024

Feng, J., Cai, R., Magliocca, E., Luo, H., Higgins, L., Romario, G. L. F., Liang, X., Pedersen, A., Xu, Z., Guo, Z., Periasamy, A., Brett, D., Miller, T. S., Haigh, S. J., Mishra, B., & Titirici, M. M. (2021). Iron, Nitrogen Co-Doped Carbon Spheres as Low Cost, Scalable Electrocatalysts for the Oxygen Reduction Reaction. *Advanced Functional Materials*,

31(46). https://doi.org/10.1002/adfm.202102974

Feng, L., Yang, L., Huang, Z., Luo, J., Li, M., Wang, D., & Chen, Y. (2013). Enhancing electrocatalytic oxygen reduction on nitrogen-doped graphene by active sites implantation. *Scientific Reports*, *3*(November). https://doi.org/10.1038/srep03306

Ficca, V. C. A., Santoro, C., Placidi, E., Arciprete, F., Serov, A., Atanassov, P., & Mecheri, B. (2023). Exchange Current Density as an Effective Descriptor of Poisoning of Active Sites in Platinum Group Metal-free Electrocatalysts for Oxygen Reduction Reaction. *ACS Catalysis*, *13*(4), 2162–2175. https://doi.org/10.1021/acscatal.2c05222

Gewirth, A. A., Varnell, J. A., & Diascro, A. M. (2018). *Nonprecious Metal Catalysts for Oxygen Reduction in Heterogeneous Aqueous Systems*. https://doi.org/10.1021/acs.chemrev.7b00335

Gong, K., Du, F., Xia, Z., Durstock, M., & Dai, L. (2009). Nitrogen-doped carbon nanotube arrays with high electrocatalytic activity for oxygen reduction. *Science*, *323*(5915), 760–764. https://doi.org/10.1126/science.1168049

He, Q., & Cairns, E. J. (2015). Review—Recent Progress in Electrocatalysts for Oxygen Reduction Suitable for Alkaline Anion Exchange Membrane Fuel Cells. *Journal of The Electrochemical Society*, *162*(14), F1504–F1539. https://doi.org/10.1149/2.0551514jes

He, W., Xiang, Y., Xin, M., Qiu, L., Dong, W., Zhao, W., Diao, Y., Zheng, A., & Xu, G. (2022). Investigation of multiple commercial electrocatalysts and electrocatalyst

degradation for fuel cells in real vehicles. *RSC Advances*, *12*(50), 32374–32382. https://doi.org/10.1039/d2ra05682h

He, X., Zheng, N., Hu, R., Hu, Z., & Yu, J. C. (2021). Hydrothermal and Pyrolytic Conversion of Biomasses into Catalysts for Advanced Oxidation Treatments. *Advanced Functional Materials*, *31*(7), 1–31. https://doi.org/10.1002/adfm.202006505

Hoshi, N., Nakamura, M., & Hitotsuyanagi, A. (2013). Active sites for the oxygen reduction reaction on the high index planes of Pt. *Electrochimica Acta*, *112*, 899–904. https://doi.org/10.1016/j.electacta.2013.05.045

Huang, J., Cao, Y., Qin, B., Zhong, G., Zhang, J., Yu, H., Wang, H., & Peng, F. (2019). Highly efficient and acid-corrosion resistant nitrogen doped magnetic carbon nanotubes for the hexavalent chromium removal with subsequent reutilization. *Chemical Engineering Journal*, *361*, 547–558. https://doi.org/10.1016/j.cej.2018.12.081

Ilkiv, B., Petrovska, S., Sergiienko, R., Foya, O., Ilkiv, O., Shibata, E., Nakamura, T., & Zaulychnyy, Y. (2015). Electronic structure of hollow graphitic carbon nanoparticles fabricated from acetylene carbon black. *Fullerenes Nanotubes and Carbon Nanostructures*, *23*(5), 449–454. https://doi.org/10.1080/1536383X.2014.885957

Inamuddin, Boddula, R., & Asiri, A. M. (2020). Methods for electrocatalysis: Advanced materials and allied applications. In *Methods for Electrocatalysis: Advanced Materials and Allied Applications* (Issue January). Springer International Publishing. https://doi.org/10.1007/978-3-030-27161-9

Jiang, W. J., Gu, L., Li, L., Zhang, Y., Zhang, X., Zhang, L. J., Wang, J. Q., Hu, J. S., Wei, Z., & Wan, L. J. (2016). Understanding the High Activity of Fe-N-C Electrocatalysts in Oxygen Reduction: Fe/Fe3C Nanoparticles Boost the Activity of Fe-Nx. *Journal of the American Chemical Society*, *138*(10), 3570–3578. https://doi.org/10.1021/jacs.6b00757

Jiménez-Ramírez, L. E., Camacho-Mojica, D. C., Muñoz-Sandoval, E., & López-Urías, F. (2017). First-principles study of transition metal adsorbed on porphyrin-like motifs in pyrrolic nitrogen-doped carbon nanostructures. *Carbon*, *116*, 381–390. https://doi.org/10.1016/j.carbon.2017.02.018

Jin, L., Zhu, B., Wang, X., Zhang, L., Song, D., Guo, J., & Tao, H. (2020). Facile synthesis of the amorphous carbon coated Fe-N-C nanocatalyst with efficient activity for oxygen reduction reaction in acidic and alkaline media. *Materials*, *13*(20), 1–16. https://doi.org/10.3390/ma13204551

Kicin, W., & Szala, M. (2013). *Sulfur-doped porous carbons : Synthesis and applications*. *68*, 1–32. https://doi.org/10.1016/j.carbon.2013.11.004

Krishnan, S. G., White, C. E., Zeng, K., Kalarikkal, N., Ok, Y. S., Arnold, C. B., Thomas, S., & Nzihou, A. (2025). Recent developments on multi- versus single-metallic catalytic graphitisation of biocarbon: A review. *Fuel*, *396*(April), 135330. https://doi.org/10.1016/j.fuel.2025.135330

Kulkarni, A., Siahrostami, S., Patel, A., & Nørskov, J. K. (2018). Understanding Catalytic Activity Trends in the Oxygen Reduction Reaction. *Chemical Reviews*, *118*(5), 2302–

2312. https://doi.org/10.1021/acs.chemrev.7b00488

Kumar, A., Khandelwal, M., Gupta, S. K., Kumar, V., & Rani, R. (2019). Fourier transform infrared spectroscopy: Data interpretation and applications in structure elucidation and analysis of small molecules and nanostructures. In *Data Processing Handbook for Complex Biological Data Sources*. Elsevier Inc. https://doi.org/10.1016/B978-0-12-816548-5.00006-X

Laursen, A. B., Man, I. C., Trinhammer, O. L., Rossmeisl, J., & Dahl, S. (2011). The Sabatier principle illustrated by catalytic H2O2 decomposition on metal surfaces. *Journal of Chemical Education*, *88*(12), 1711–1715. https://doi.org/10.1021/ed101010x

Lee, S. H., Kim, J., Chung, D. Y., Yoo, J. M., Lee, H. S., Kim, M. J., Mun, B. S., Kwon, S. G., Sung, Y. E., & Hyeon, T. (2019). Design Principle of Fe-N-C Electrocatalysts: How to Optimize Multimodal Porous Structures? *Journal of the American Chemical Society*, *141*(5), 2035–2045. https://doi.org/10.1021/jacs.8b11129

Lefevre, M., Dodelet, J. P., & Bertrand, P. (2000). O2 reduction in PEM fuel cells: Activity and active site structural information for catalysts obtained by the pyrolysis at high temperature of Fe precursors. *Journal of Physical Chemistry B*, *104*(47), 11238–11247. https://doi.org/10.1021/jp002444n

Lei, H., Zhang, Q., Liang, Z., Guo, H., Wang, Y., Lv, H., Li, X., Zhang, W., Apfel, U. P., & Cao, R. (2022). Metal-Corrole-Based Porous Organic Polymers for Electrocatalytic Oxygen Reduction and Evolution Reactions. *Angewandte Chemie - International Edition*, *61*(24). https://doi.org/10.1002/anie.202201104

Li, Y., Liu, T., Yang, W., Zhu, Z., Zhai, Y., Gu, W., & Zhu, C. (2019a). Multiscale porous Fe-N-C networks as highly efficient catalysts for the oxygen reduction reaction. *Nanoscale*, *11*(41), 19506–19511. https://doi.org/10.1039/c9nr05726a

Li, Y., Liu, T., Yang, W., Zhu, Z., Zhai, Y., Gu, W., & Zhu, C. (2019b). Multiscale porous Fe-N-C networks as highly efficient catalysts for the oxygen reduction reaction. *Nanoscale*, *11*(41), 19506–19511. https://doi.org/10.1039/c9nr05726a

Liang, H. W., Zhuang, X., Brüller, S., Feng, X., & Müllen, K. (2014). Hierarchically porous carbons with optimized nitrogen doping as highly active electrocatalysts for oxygen reduction. *Nature Communications*, *5*(September). https://doi.org/10.1038/ncomms5973

Lilloja, J., Mooste, M., Kibena-Põldsepp, E., Sarapuu, A., Zulevi, B., Kikas, A., Piirsoo, H. M., Tamm, A., Kisand, V., Holdcroft, S., Serov, A., & Tammeveski, K. (2021). Mesoporous iron-nitrogen co-doped carbon material as cathode catalyst for the anion exchange membrane fuel cell. *Journal of Power Sources Advances*, *8*(February). https://doi.org/10.1016/j.powera.2021.100052

Liu, H., Zhao, J., & Li, X. (2022). Controlled Synthesis of Carbon-Supported Pt-Based Electrocatalysts for Proton Exchange Membrane Fuel Cells. In *Electrochemical Energy Reviews* (Vol. 5, Issue 4). Springer Nature Singapore. https://doi.org/10.1007/s41918-022-00173-3

Liu, J., Fan, C., Liu, G., & Jiang, L. (2021). MOF-derived dual metal (Fe, Ni)–nitrogen–doped carbon for synergistically enhanced oxygen reduction reaction. *Applied Surface*

Science, *538*, 148017. https://doi.org/10.1016/j.apsusc.2020.148017

Liu, Q., Duan, Y., Zhao, Q., Pan, F., Zhang, B., & Zhang, J. (2014). Direct synthesis of nitrogen-doped carbon nanosheets with high surface area and excellent oxygen reduction performance. *Langmuir*, *30*(27), 8238–8245. https://doi.org/10.1021/la404995y

Maboya, W. K., Maubane-Nkadimeng, M. S., Jijana, A. N., & Mmako, H. K. (2022). Nitrogen inclusion in carbon nanotubes initiated by boron doping and chlorination: Their use as electrocatalysts for oxygen reduction reaction. *Frontiers in Materials*, *9*(December), 1–14. https://doi.org/10.3389/fmats.2022.886471

Masa, J., Xia, W., Muhler, M., & Schuhmann, W. (2015). *On the Role of Metals in Nitrogen-Doped Carbon Electrocatalysts for Oxygen Reduction Angewandte*. 10102–10120. https://doi.org/10.1002/anie.201500569

Masa, J., Xia, W., Sinev, I., Zhao, A., Sun, Z., Grützke, S., Weide, P., Muhler, M., & Schuhmann, W. (2014). *Angewandte MnxOy/NC and CoxOy/NC Nanoparticles Embedded in a Nitrogen-Doped Carbon Matrix for High-Performance Bifunctional Oxygen Electrodes*. **. 8508–8512. https://doi.org/10.1002/anie.201402710

Masa, J., Zhao, A., Xia, W., Muhler, M., & Schuhmann, W. (2013). Metal-free catalysts for oxygen reduction in alkaline electrolytes: Influence of the presence of Co, Fe, Mn and Ni inclusions. *Electrochimica Acta*. https://doi.org/10.1016/j.electacta.2013.11.026

Masa, J., Zhao, A., Xia, W., Sun, Z., Mei, B., Muhler, M., & Schuhmann, W. (2013).

Electrochemistry Communications Trace metal residues promote the activity of supposedly metal-free nitrogen-modified carbon catalysts for the oxygen reduction reaction. *Electrochemistry Communications*, *34*, 113–116. https://doi.org/10.1016/j.elecom.2013.05.032

Mbokazi, S. P., Matthews, T., Chabalala, M. P., Zikhali, M., Mugadza, K., Gwebu, S., Maxakato, N. W., Zheng, H., & Mekuto, L. (2024). Elucidating the effects of nitrogen and phosphorus co-doped carbon on complex spinel NiFe2O4 towards oxygen reduction reaction in alkaline media. *Heliyon*, *10*(15), e35483. https://doi.org/10.1016/j.heliyon.2024.e35483

Mehmood, A., Ali, B., Gong, M., Gyu Kim, M., Kim, J. Y., Bae, J. H., Kucernak, A., Kang, Y. M., & Nam, K. W. (2021). Development of a highly active Fe–N–C catalyst with the preferential formation of atomic iron sites for oxygen reduction in alkaline and acidic electrolytes. *Journal of Colloid and Interface Science*, *596*, 148–157. https://doi.org/10.1016/j.jcis.2021.03.081

Meyer, Q., Zeng, Y., & Zhao, C. (2019). Electrochemical impedance spectroscopy of catalyst and carbon degradations in proton exchange membrane fuel cells. *Journal of Power Sources*, *437*(July), 226922. https://doi.org/10.1016/j.jpowsour.2019.226922

Mi, X., Gao, B., Tan, X., Xie, M., & Gao, C. (2020). ScienceDirect Preparation of iron and nitrogen co-doped carbon material Fe / N-C CM-T for oxygen reduction reaction. *International Journal of Hydrogen Energy*, *xxxx*. https://doi.org/10.1016/j.ijhydene.2020.11.057

Miao, S., Liang, K., Zhu, J., Yang, B., Zhao, D., & Kong, B. (2020). Nano Today Hetero-atom-doped carbon dots : Doping strategies , properties and applications. *Nano Today*, *33*, 100879. https://doi.org/10.1016/j.nantod.2020.100879

Osikoya, A. O., Wankasi, D., Vala, R. M. K., Dikio, C. W., Afolabi, A. O., Ayawei, N., & Dikio, E. D. (2015). Synthesis, characterization and sorption studies of nitrogen–doped carbon nanotubes. *Digest Journal of Nanomaterials and Biostructures*, *10*(1), 125–134.

Osmieri, L., Cullen, D. A., Chung, H. T., Ahluwalia, R. K., & Neyerlin, K. C. (2020). Durability evaluation of a Fe–N–C catalyst in polymer electrolyte fuel cell environment via accelerated stress tests. *Nano Energy*, *78*, 1–30. https://doi.org/10.1016/j.nanoen.2020.105209

Park, M. J., Lee, J. H., Hembram, K. P. S. S., Lee, K. R., Han, S. S., Yoon, C. W., Nam, S. W., & Kim, J. Y. (2016). Oxygen reduction electrocatalysts based on coupled iron nitride nanoparticles with nitrogen-doped carbon. *Catalysts*, *6*(6). https://doi.org/10.3390/catal6060086

Parvez Ahmad, M. D., Venkateswara Rao, A., Suresh Babu, K., & Narsinga Rao, G. (2020). Effect of carbon-doping on structural and dielectric properties of zinc oxide. *Journal of Advanced Dielectrics*, *10*(4), 1–7. https://doi.org/10.1142/S2010135X20500174

Peng, H., Mo, Z., Liao, S., Liang, H., Yang, L., Luo, F., Song, H., Zhong, Y., & Zhang, B. (2013). High performance Fe- and N- Doped carbon catalyst with graphene structure for oxygen reduction. *Scientific Reports*, *3*, 1–7. https://doi.org/10.1038/srep01765

Petrii, O. A., & Tsirlina, G. A. (1994). Electrocatalytic activity prediction for hydrogen electrode reaction: intuition, art, science. *Electrochimica Acta*, *39*(11–12), 1739–1747. https://doi.org/10.1016/0013-4686(94)85159-X

Rameshaiah, G. N., & Ashoka, H. (2015). Caffeine Extraction and Characterization. *Int J Cur Res Rev*, *7*(9), 16–19. https://www.researchgate.net/publication/326293350

Reactions, O. E. (2019). *Novel Non-Precious Metal Electrocatalysts for Oxygen Electrode Reactions*. 15–17.

Serhan, M., Sprowls, M., Jackemeyer, D., Long, M., Perez, I. D., Maret, W., Tao, N., & Forzani, E. (2019). Total iron measurement in human serum with a smartphone. *AIChE Annual Meeting, Conference Proceedings*, *2019-Novem*. https://doi.org/10.1039/x0xx00000x

Shah, R. K. (2007). Introduction to fuel cells. *Recent Trends in Fuel Cell Science and Technology*, *877*, 1–9. https://doi.org/10.1007/978-0-387-68815-2_1

Shao, M., Chang, Q., Dodelet, J. P., & Chenitz, R. (2016). Recent Advances in Electrocatalysts for Oxygen Reduction Reaction. *Chemical Reviews*, *116*(6), 3594–3657. https://doi.org/10.1021/acs.chemrev.5b00462

Sharma, S. K., Verma, D. S., Khan, L. U., Kumar, S., & Khan, S. B. (2018). Handbook of Materials Characterization. *Handbook of Materials Characterization*, *July 2020*, 1–613. https://doi.org/10.1007/978-3-319-92955-2

Shen, H., Thomas, T., Rasaki, S. A., Saad, A., Hu, C., Wang, J., & Yang, M. (2019). Oxygen

Reduction Reactions of Fe-N-C Catalysts: Current Status and the Way Forward. *Electrochemical Energy Reviews*, *2*(2), 252–276. https://doi.org/10.1007/s41918-019-00030-w

Shen, S., Jiang, W., Zhao, Q., He, L., Ma, Y., Zhou, X., Wang, J., Yang, L., & Chen, Z. (2023). Molten-salts assisted preparation of iron-nitrogen-carbon catalyst for efficient degradation of acetaminophen by periodate activation. *Science of the Total Environment*, *859*(September 2022), 160001. https://doi.org/10.1016/j.scitotenv.2022.160001

Shen, T. Y., Jia, P. Y., Chen, D. S., & Wang, L. N. (2021). Hydrothermal synthesis of N-doped carbon quantum dots and their application in ion-detection and cell-imaging. *Spectrochimica Acta - Part A: Molecular and Biomolecular Spectroscopy*, *248*, 119282. https://doi.org/10.1016/j.saa.2020.119282

Shi, S., Wang, Y., Wang, B., Wu, F., Suo, Y., Zhang, Z., & Xu, Y. (2022). Cobalt, sulfur, nitrogen co-doped carbon as highly active electrocatalysts towards oxygen reduction reaction. *International Journal of Hydrogen Energy*, *47*(92), 39058–39069. https://doi.org/https://doi.org/10.1016/j.ijhydene.2022.09.073

Shilpa, Kumar, R., & Sharma, A. (2018). Morphologically tailored activated carbon derived from waste tires as high-performance anode for Li-ion battery. *Journal of Applied Electrochemistry*, *48*(1), 1–13. https://doi.org/10.1007/s10800-017-1129-3

Shinagawa, T., Garcia-esparza, A. T., & Takanabe, K. (2015). Insight on Tafel slopes from a microkinetic analysis of aqueous electrocatalysis for energy conversion. *Nature*

Publishing Group, *August*, 1–21. https://doi.org/10.1038/srep13801

Strbac, S. (2021). The effect of pH on oxygen and hydrogen peroxide reduction on polycrystalline Pt electrode Electrochimica Acta The effect of pH on oxygen and hydrogen peroxide reduction on polycrystalline Pt electrode. *Electrochimica Acta*, *56*(3), 1597–1604. https://doi.org/10.1016/j.electacta.2010.10.057

Strelko, V. V., Kuts, V. S., & Thrower, P. A. (2000). On the mechanism of possible influence of heteroatoms of nitrogen, boron and phosphorus in a carbon matrix on the catalytic activity of carbons in electron transfer reactions. *Carbon*, *38*(10), 1499–1503. https://doi.org/10.1016/S0008-6223(00)00121-4

Strickland, K., Li, J., Serov, A., Artyushkova, K., Atanassov, P., Gumeci, C., Barton, S. C., Sougrati, M., Jaouen, F., & Mukerjee, S. (2016). Author ' s Accepted Manuscript Spectroscopic Insights into the Nature of Active Sites in Iron-Nitrogen-Carbon Electrocatalysts for Oxygen Reduction in Acid and the Redox Mechanisms. *Nano Energy*. https://doi.org/10.1016/j.nanoen.2016.03.025

Sun, Y., Du, C., An, M., Du, L., Tan, Q., Liu, C., Gao, Y., & Yin, G. (2015). Boron-doped graphene as promising support for platinum catalyst with superior activity towards the methanol electrooxidation reaction. *Journal of Power Sources*, *300*, 245–253. https://doi.org/10.1016/j.jpowsour.2015.09.046

Sustainable, T., & Goals, D. (2021). *The Sustainable Development Goals Report*.

Tang, H., Qiu, T., Wang, X., Zhang, C., & Zhang, Z. (2024). A Brief Review of Recent

Theoretical Advances in Fe-Based Catalysts for CO2 Hydrogenation. *Molecules*, *29*(6). https://doi.org/10.3390/molecules29061194

Tohnoe, M., Matsuda, R., Kai, S., & Imasaki, M. (1989). Nonlinear effect in ferroelectric liquid crystal 8s1* due to interfacial interaction with substrates. *Ferroelectrics*, *96*(1), 263–267. https://doi.org/10.1080/00150198908216783

Van Ede, M. C., & Angst, U. (2023). *Tafel slopes and exchange current densities of oxygen reduction and hydrogen evolution on steel: influence of the electrochemical measurement procedure*. 1–24.

Vij, V., Tiwari, J. N., Lee, W. G., Yoon, T., & Kim, K. S. (2016). Hemoglobin-carbon nanotube derived noble-metal-free Fe5C2-based catalyst for highly efficient oxygen reduction reaction. *Scientific Reports*, *6*(February), 2–10. https://doi.org/10.1038/srep20132

Volperts, A., Upskuviene, D., Balciunaite, A., Jasulaitiene, V., Niaura, G., Drabavicius, A., Plavniece, A., Dobele, G., Zhurinsh, A., Lin, Y. C., Chen, Y. W., Tamasauskaite-Tamasiunaite, L., & Norkus, E. (2023). Copper-nitrogen dual-doped activated carbon derived from alder wood as an electrocatalyst for oxygen reduction. *Catalysis Communications*, *182*(July), 106743. https://doi.org/10.1016/j.catcom.2023.106743

Wang, J., Zhao, C., Liu, J., Ren, D., Li, B., Huang, J., & Zhang, Q. (2021a). Nano Materials Science Quantitative kinetic analysis on oxygen reduction reaction : A perspective. *Nano Materials Science*, *3*(3), 313–318. https://doi.org/10.1016/j.nanoms.2021.03.006

Wang, J., Zhao, C. X., Liu, J. N., Ren, D., Li, B. Q., Huang, J. Q., & Zhang, Q. (2021b). Quantitative kinetic analysis on oxygen reduction reaction: A perspective. *Nano Materials Science*, *3*(3), 313–318. https://doi.org/10.1016/j.nanoms.2021.03.006

Wang, S., Zhang, J., Gharbi, O., Vivier, V., Gao, M., & Orazem, M. E. (2021). Electrochemical impedance spectroscopy. *Nature Reviews Methods Primers*, *1*(1). https://doi.org/10.1038/s43586-021-00039-w

Wang, X., Li, Z., Qu, Y., Yuan, T., Wang, W., Wu, Y., & Li, Y. (2019). Review of Metal Catalysts for Oxygen Reduction Reaction: From Nanoscale Engineering to Atomic Design. *Chem*, *5*(6), 1486–1511. https://doi.org/10.1016/j.chempr.2019.03.002

Wang, X., Yang, X., Chen, C., Li, H., Huang, Y., & Cao, R. (2022). Graphene Quantum Dots Supported on Fe-based Metal-Organic Frameworks for Efficient Photocatalytic CO2 Reduction. *Acta Chimica Sinica*, *80*(1), 22–28. https://doi.org/10.6023/A21100455

Wang, Y., Nian, Y., Biswas, A. N., Li, W., Han, Y., & Chen, J. G. (2021). Challenges and Opportunities in Utilizing MXenes of Carbides and Nitrides as Electrocatalysts. *Advanced Energy Materials*, *11*(3), 1–17. https://doi.org/10.1002/aenm.202002967

Wei, Q., Tong, X., Zhang, G., Qiao, J., Gong, Q., & Sun, S. (2015). Nitrogen-doped carbon nanotube and graphene materials for oxygen reduction reactions. *Catalysts*, *5*(3), 1574–1602. https://doi.org/10.3390/catal5031574

Weiss, J., Zhang, H., & Zelenay, P. (2020). Recent progress in the durability of Fe-N-C oxygen reduction electrocatalysts for polymer electrolyte fuel cells. *Journal of*

Electroanalytical Chemistry, *875*, 114696. https://doi.org/10.1016/j.jelechem.2020.114696

Wiggins-Camacho, J. D., & Stevenson, K. J. (2011). Mechanistic discussion of the oxygen reduction reaction at nitrogen-doped carbon nanotubes. *Journal of Physical Chemistry C*, *115*(40), 20002–20010. https://doi.org/10.1021/jp205336w

Wood, P. M. (1988). The potential diagram for oxygen at pH 7. *Biochemical Journal*, *253*(1), 287–289. https://doi.org/10.1042/bj2530287

Wu, G., & Zelenay, P. (2013). Nanostructured nonprecious metal catalysts for oxygen reduction reaction. *Accounts of Chemical Research*, *46*(8), 1878–1889. https://doi.org/10.1021/ar400011z

Wu, Z., Iqbal, Z., & Wang, X. (2015). Metal-free, carbon-based catalysts for oxygen reduction reactions. *Frontiers of Chemical Science and Engineering*, *9*(3), 280–294. https://doi.org/10.1007/s11705-015-1524-4

Xia, W., Masa, J., Bron, M., Schuhmann, W., & Muhler, M. (2011). Highly active metal-free nitrogen-containing carbon catalysts for oxygen reduction synthesized by thermal treatment of polypyridine-carbon black mixtures. *Electrochemistry Communications*, *13*(6), 593–596. https://doi.org/10.1016/j.elecom.2011.03.018

Xu, S., Zhang, S., Li, Y., & Liu, J. (2023). Facile Synthesis of Iron and Nitrogen Co-Doped Carbon Dot Nanozyme as Highly Efficient Peroxidase Mimics for Visualized Detection of Metabolites. *Molecules*, *28*(16). https://doi.org/10.3390/molecules28166064

Yang, T., Chen, Y., Liu, Y., Liu, X., & Gao, S. (2022). Self-sacrificial template synthesis of Fe, N co-doped porous carbon as efficient oxygen reduction electrocatalysts towards Zn-air battery application. *Chinese Chemical Letters*, *33*(4), 2171–2177. https://doi.org/10.1016/j.cclet.2021.09.014

Yeager, E. (1984). Electrocatalysts for O2 reduction. *Electrochimica Acta*, *29*(11), 1527–1537. https://doi.org/10.1016/0013-4686(84)85006-9

Zagal, J., Bindra, P., & Yeager, E. (1980). A Mechanistic Study of O 2 Reduction on Water Soluble Phthalocyanines Adsorbed on Graphite Electrodes. *Journal of The Electrochemical Society*, *127*(7), 1506–1517. https://doi.org/10.1149/1.2129940

Zhang, C., Fan, F. R. F., & Bard, A. J. (2009). Electrochemistry of oxygen in concentrated NaOH solutions: Solubility, diffusion coefficients, and superoxide formation. *Journal of the American Chemical Society*, *131*(1), 177–181. https://doi.org/10.1021/ja8064254

Zhang, L., Hu, Y., Jiang, K., Li, K., Liu, Y.-Q., Wang, D., & Ye, Y. (2021). The Role of Sulfur Doping in Determining the Performance of Fe/N-C Based Electrocatalysts for Oxygen Reduction Reactions. *Journal of The Electrochemical Society*, *168*(5), 054523. https://doi.org/10.1149/1945-7111/ac0065

Zhao, A., Masa, J., Muhler, M., Schuhmann, W., & Xia, W. (2013). Electrochimica Acta N-doped carbon synthesized from N-containing polymers as metal-free catalysts for the oxygen reduction under alkaline conditions. *Electrochimica Acta*, *98*, 139–145. https://doi.org/10.1016/j.electacta.2013.03.043

Zhao, A., Masa, J., Schuhmann, W., & Xia, W. (2013). *Activation and Stabilization of Nitrogen-Doped Carbon Nanotubes as Electrocatalysts in the Oxygen Reduction Reaction at Strongly Alkaline Conditions*.

Zhao, L., Zhang, Y., Huang, L. B., Liu, X. Z., Zhang, Q. H., He, C., Wu, Z. Y., Zhang, L. J., Wu, J., Yang, W., Gu, L., Hu, J. S., & Wan, L. J. (2019). Cascade anchoring strategy for general mass production of high-loading single-atomic metal-nitrogen catalysts. *Nature Communications*, *10*(1). https://doi.org/10.1038/s41467-019-09290-y

Zhao, Y. M., Yu, G. Q., Wang, F. F., Wei, P. J., & Liu, J. G. (2019). Bioinspired Transition-Metal Complexes as Electrocatalysts for the Oxygen Reduction Reaction. *Chemistry - A European Journal*, *25*(15), 3726–3739. https://doi.org/10.1002/chem.201803764

Zhou, Y., Chen, G., & Zhang, J. (2020). A review of advanced metal-free carbon catalysts for oxygen reduction reactions towards the selective generation of hydrogen peroxide. *Journal of Materials Chemistry A*, *8*(40), 20849–20869. https://doi.org/10.1039/d0ta07900f

Zou, J., Wang, B., Zhu, B., Yang, Y., Han, W., & Dong, A. (2019). Fe, N, S-codoped carbon frameworks derived from nanocrystal superlattices towards enhanced oxygen reduction activity. *Nano Convergence*, *6*(1). https://doi.org/10.1186/s40580-019-0174-5

Zou, Y., Wang, X., Khan, A., Wang, P., Liu, Y., Alsaedi, A., Hayat, T., & Wang, X. (2016). Environmental Remediation and Application of Nanoscale Zero-Valent Iron and Its Composites for the Removal of Heavy Metal Ions: A Review. *Environmental Science*

and Technology, *50*(14), 7290–7304. https://doi.org/10.1021/acs.est.6b01897

APPENDICES

Appendix 1. Koutecky-Levich analysis data for GC, OSS1 and OSS2 polarisation curve.

Sample ID	Potential (V)	n	j_K ($mAcm^{-2}$)	k (s^{-1})
OSS1	-0.380	3.000	1.145	3.295
	-0.400	2.920	1.405	4.156
	-0.450	2.920	1.858	5.496
	-0.500	2.910	2.027	6.017
	-0.433	**2.940**	**1.609**	**4.741**
	Std	**0.040**	**0.406**	**1.243**
OSS2	-0.433	3.290	1.998	5.245
	-0.450	3.270	2.139	5.650
	-0.480	3.200	2.283	6.162
	-0.500	3.190	2.335	6.323
	-0.466	**3.240**	**2.189**	**5.845**
	Std	**0.043**	**0.132**	**0.426**
GC	-0.300	2.300	0.634	2.380
	-0.295	2.290	0.916	3.453
	-0.290	2.300	1.075	4.037
	-0.280	2.630	1.405	4.614
	-0.290	**2.380**	**1.007**	**3.621**
	Std	**0.170**	**0.322**	**0.953**

Appendix 2. Tafel slope analysis for GC, OSS1 and OSS2.

Sample ID	Speed (rpm)	Slope	a (mAcm-2)	α
GC	100	-99.240	0.361	0.071
	400	-95.340	0.354	0.073
	900	-94.010	0.350	0.073
	1600	-95.100	0.349	0.074
	Mean	**-95.920**	**0.354**	**0.073**
	Std	**2.290**	**0.006**	**0.001**
OSS1	100	-107.830	0.357	0.072
	400	-103.530	0.350	0.073
	900	-101.940	0.346	0.074
	1600	-101.120	0.345	0.074
	Mean	**-103.610**	**0.350**	**0.073**
	Std	**2.990**	**0.005**	**0.001**
OSS2	100	-118.860	0.501	0.051
	400	-114.580	0.467	0.055
	900	-112.990	0.438	0.059
	1600	-112.155	0.428	0.060
	Mean	**-114.650**	**0.459**	**0.0562**
	Std	**2.980**	**0.033**	**0.004**